Advances in Nano Research, *Vol. 12, No. 3 (2022) 231-251*
https://doi.org/10.12989/anr.2022.12.3.231

Dynamic analysis of functionally graded (FG) nonlocal strain gradient nanobeams under thermo-magnetic fields and moving load

Mashhour A. Alazwari[1a], Ismail Esen[2], Alaa A. Abdelrahman[3], Azza M. Abdraboh[4] and Mohamed A. Eltaher[*1,3]

[1]*Mechanical Engineering Dept., Faculty of Engineering, King Abdulaziz University, P.O. Box 80204, Jeddah, Saudi Arabia*
[2]*Department of Mechanical Engineering, Karabuk University, Karabuk, Turkey*
[3]*Mechanical Design and Prod. Dept., Faculty of Engineering, Zagazig University, P.O. Box 44519, Zagazig, Egypt*
[4]*Physics Department, Faculty of Science, Benha University, Benha, Egypt*

(*Received September 8, 2020, Revised October 12, 2021, Accepted October 13, 2021*)

Abstract. Dynamic behavior of temperature-dependent Reddy functionally graded (RFG) nanobeam subjected to thermomagnetic effects under the action of moving point load is carried out in the present work. Both symmetric and sigmoid functionally graded material distributions throughout the beam thickness are considered. To consider the significance of strain-stress gradient field, a material length scale parameter (LSP) is introduced while the significance of nonlocal elastic stress field is considered by introducing a nonlocal parameter (NP). In the framework of the nonlocal strain gradient theory (NSGT), the dynamic equations of motion are derived through Hamilton's principle. Navier approach is employed to solve the resulting equations of motion of the functionally graded (FG) nanoscale beam. The developed model is verified and compared with the available previous results and good agreement is observed. Effects of through-thickness variation of FG material distribution, beam aspect ratio, temperature variation, and magnetic field as well as the size-dependent parameters on the dynamic behavior are investigated. Introduction of the magnetic effect creates a hardening effect; therefore, higher values of natural frequencies are obtained while smaller values of the transverse deflections are produced. The obtained results can be useful as reference solutions for future dynamic and control analysis of FG nanobeams reinforced nanocomposites under thermomagnetic effects.

Keywords: higher-order shear theory; moving point load; nonlocal strain gradient nanobeams; symmetric and sigmoid FG; thermo-magnetic analysis; temperature-dependent material

1. Introduction

The growth of utilizing nanotechnology has led to expanding the interest in micromechanical modeling, Abdelrahman *et al*. (2021a, b). For dynamic analysis, Barati *et al*. (2019) involved the hydrothermal influence on the dynamic response of NSGT nanostructure beam using analytical methods. Based on higher-order shear deformation theory, Ebrahimi and Barati (2018) studied the vibration of actuated nonlocal nanobeam under magneto-electrical field and exposed to thermal environment. Safaei *et al*. (2019) investigated the free vibration behavior of polyethylene/carbo nanotube (CNTs) plates. Azrar *et al*. (2019) analyzed numerically the dynamic instability of magneto-electro-elastic beams under static/dynamic electric and magnetic fields. In accordance with NSGT, Jalaei *et al*. (2019) studied the dynamic instability behavior of FG nanobeam under an axial load and exposed to a magnetic-thermal environment. Jalaei and Civalek (2019) investigated the dynamic of viscoelastic graphene sheet under periodic axial load including thermal effects using nonlocal strain gradient theory. Barati *et al*. (2020) studied the transverse vibrations of 2D FG nonlocal nanobeams under a longitudinal magnetic field by using the modified differential quadrature method. Alizadeh *et al*. (2020) exploited the Laplace method to study vibration of the gold microbeam resonator considering the thermoelastic damping and Green-Naghdi thermo-elasticity theory. Eltaher and Mohamed (2020) presented the free vibration and instability response of curved carbon nanotube by using doublet mechanics theory to include the size-dependency effect.

Ahn and Rail (2021) investigated the one-dimensional frictional contact problems including thermal effects based on standard linear beams. Assie *et al*. (2021) studied the vibration response of perforated thick Timoshenko beam under moving load by using the Ritz method. Esen *et al*. (2021 a, b) predicted the mechanical response of FG Timoshenko microbeam and free vibration of cracked FG nonlocal Euler nanobeam embedded rested on elastic matrix and exposed to thermo-magnetic environment. Devarajan (2021) used isogeometric analysis to study the free vibration of curvilinearly stiffened laminated composite perforated plates. Lal and Dangi (2021) presented the free vibration of 2D FG thick nonlocal nanobeam under the influence of surface effect.

Recognizing and influencing the motion of nano-particles is critical for micro- and nano-assembly, micro-fluidics, including biological and colloidal science applications, chemical mechanical polishing, and xero-

*Corresponding author, Professor,
E-mail: meltaher@kau.edu.sa
[a] Ph.D., E-mail: maalazwari@kau.edu.sa

ISSN: 2287-237X (Print), 2287-2388 (Online)

graphic processes, Eglin *et al*. (2006). Such as, nanotubes and nanobeams may be used to transport drug materials into targeted nano-sized molecules to change the behaviour of cancer cells, Roudbari *et al*. (2020).

Yayli (2015a, b, 2016a, b) studied the buckling of strain gradient nanobeam and longitudinal vibration of hardening nonlocal nanorods under different boundary conditions. Yayli (2018 a, b, c) investígated torsional vibration of nonlocal nanorods with elastic torsional restraints, nonlocal nanotube embbeded in elastic médium, and torisnal nanotube base don modified couple stress theory. Barati (2017) developed NSGT to analyze vibration of porous FG nanobeams under moving nanosize mass. Arefi *et al*. (2018) predicted the vibration behavior of FG microbeam resting on elastic foundations under moving mass. Rajasekaran and Khaniki (2019) inspected a vibration response of 2D FG microbeam with variable elastic foundation under moving mass. Yayli (2019) presented the influance of rotational restraints on the thermal buckling of CNTs. Esen *et al*. (2020a) explored the dynamic response of perforated Timoshenko modified couple stress microbeams under moving loads using the finite element method. Jazi (2020) studied nonlinear forced vibration response of elastically connected double nanobeams subjected to a moving particle in the framework of modified couple stress theory. Zhang *et al*. (2021) predicted the snap-buckling of FG-CNTR curved nanobeams with surface energy. Esen *et al*. (2021c) studied the dynamic response of symmetrical and sigmoidal FG Timoshenko beam rested on an elastic foundation under the influence of moving point mass. Lu *et al*. (2021a, b) and She *et al*. (2021a) presented size-dependent influences on postbuckling, free vibration, and resonances of imperfected graphene reinforced composite microtubes. Esen (2021d) exploited the nonlocal strain gradient theory to study the dynamic behaviors of FG nanobeam reinforced by CNTs under moving point load. She *et al*. (2021b) studied the eave propagation of FG plate under a thermal loads. Abdelrahman *et al*. (2021a) used a modified nonlocal strain gradient Timoshenko continuum model to study the size and microstructure influences on the vibration response of perforated nanobeams under moving dynamic loads. Ding and She (2021) explored the snap-buckling of FG pipes conveying fluid using higher order shear theory. Abdelrahman *et al*. (2021b, c) presented the influences of perforation parameters, thermal loading profile, size scale, and speed of moving mass on the vibration amplitudes of microbeams with perforation.

Based on the previous works and knowledge of authors, the dynamic analysis and vibration time response of functionally graded nanobeams under both thermal and magnetic fields and subjected to moving load has not been discussed before. Therefore, the current study aims to fill this gap by presenting an analytical methodology to study and analyze free and forced vibration behavior of functionally graded higher-order shear deformation nano-beams in thermomagnetic fields under moving load. The following article has been ordered as, the theory and formulation, kinematic relation, constitutive equations of macro and microstructure, and governing equations of motion are discussed in section 2. The analytical solution methodology is derived in section 3. verification of the present model with previous work has been proved in section 4. In section 5, the numerical results and parametric studies have been discussed in detail through this section. Most findings and summarized discussion have been highlighted in the conclusion section.

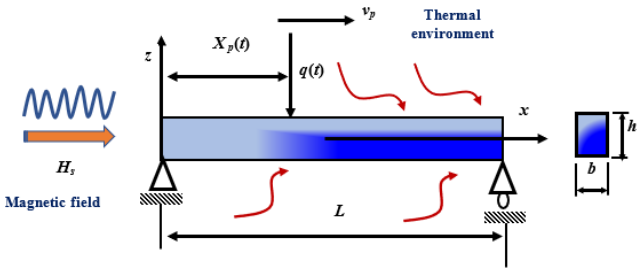

Fig. 1 The geometry of functionally graded beam exposed to a magnetic field in a thermal environment under moving load

2. Theory and formulation

2.1 Functionally graded material model

Consider a functionally graded nanobeam shown in Fig. 1. The beam is exposed to a point moving load and magnetic field in a thermal environment. It is assumed that the material ingredients vary, in a continuous and smooth manner, throughout the beam thickness direction. According to the Voigt model, the volume fraction at any point through the thickness can be expressed as Hamed *et al*. (2016, 2019). The power-law form is adopted to evaluate the material distribution throughout the beam thickness. The effective material properties can be given by Attia and Abdelrahman (2018):

$$P_{ef} = P_c V_c + P_m V_m \tag{1}$$

Here, P_c and P_m are respectively referring to the specific material properties of the ceramic and metal and the volume fractions V_c and V_m are defined as follows Attia and Abdelrahman (2018):

$$V_c(z) = \left(\frac{z}{h} + \frac{1}{2}\right)^k, \; V_c(z) + V_m(z) = 1 \tag{2}$$

where k ($k \geq 0$) is the power-law index refers to the material variation throughout the thickness direction z. While $V(z)$ refers to the volume fraction of constituents and k is the exponent index that controls the material distribution.

The influence of the functionally graded material distribution through the thickness direction is investigated by considering different types of distributions. Symmetric power (SP-MCM and SP-CMC) and sigmoid functions are considered. In the symmetric power (SP) ceramic-metal-ceramic (CMC) type, the material gradation through the thickness of the beam can be depicted by, Hamed *et al*. (2016) and Avcar (2019).

SP-CMC

$$P(z) = P_m + (P_c - P_m)\left(\frac{-2z}{h}\right)^k \quad \left(-\frac{h}{2} \leq z \leq 0\right)$$
$$P(z) = P_m + (P_c - P_m)\left(\frac{2z}{h}\right)^k \quad \left(0 \leq z \leq \frac{h}{2}\right) \tag{3}$$

Table 1 Temperature-dependent coefficients for the properties of Si_3N_4, SUS304, and Ti-6Al-4V (Reddy and Chin 1998, Touloukian 1966)

Material	Property	P_{-1}	P_0	P_1	P_2	P_3	$P(T$=300**K**$)$
Si_3N_4	E (Pa)	0	348.43e + 9	-3.070e-4	2.160e-7	-8.946e-11	3.2227e+11
	υ	0	0.24	0	0	0	0.24
	α (1**K**$^{-1}$)	0	5.8723e-6	9.095e-4	0	0	7.4746e-06
	ρ (kg/m^3)	0	2370	0	0	0	2370
SUS304	E (Pa)	0	201.04e+9	3.079e-4	-6.534e-7	0	207.7877 e+9
	υ	0	0.3262	-2.002e-4	3.97e-7	0	0.3177
	α (1K^{-1})	0	12.33e-6	8.086e-4	0	0	15.32e-6
	ρ (kg/m^3)	0	8166	0	0	0	8166
Ti-6Al-4V	E (Pa)	0	122.56e+9	-4.586e-4	0	0	1.0570e+11
	υ	0	0.2884	1.121e-4	0	0	0.2981
	α (1K^{-1})	0	7.5788e-6	6.638e-4	-3.147e-6	0	6.9415e-06
	ρ (kg/m^3)	0	4512	0	0	0	4512

where P is the material properties, such as elasticity modulus (E), mass density (ρ), and Poisson's ratio (ν). The symmetric power metal-ceramic-metal (SP-MCM) functionally graded material model can be given by

SP-MCM

$$P(z) = P_c + (P_m - P_c)\left(\frac{-2z}{h}\right)^k \quad \left(-\frac{h}{2} \le z \le 0\right)$$
$$P(z) = P_c + (P_m - P_c)\left(\frac{2z}{h}\right)^k \quad \left(0 \le z \le \frac{h}{2}\right) \tag{4}$$

The sigmoid functionally graded material model is expressed as, Melaibari *et al*. (2020)

Sigmoid

$$P(z) = P_m + \frac{1}{2}(P_c - P_m)\left(1 + \frac{2z}{h}\right)^n \quad \left(-\frac{h}{2} \le z \le 0\right)$$
$$P(z) = P_c + \frac{1}{2}(P_m - P_c)\left(1 - \frac{2z}{h}\right)^n \quad \left(0 \le z \le \frac{h}{2}\right) \tag{5}$$

The temperature dependency of the FG material properties are assumed to be nonlinear and given by the following nonlinear relation, Touloukian (1966):

$$P = P_0(P_{-1}T^{-1} + 1 + P_1T + P_2T^2 + P_3T^3) \tag{6}$$

Here, as given in Table 1, P_0, P_{-1}, P_1, P_2, and P_3 are the specific temperature (T, K) dependent material coefficients, where $= T_0 + \Delta T$, $T_0 = 300K$, ΔT is the uniform temperature rise. Note that the other linear and nonlinear temperature distributions along the thickness are not considered in this study. One can refer to Esen (2019), Ebrahimi and Barati (2016a, b) for the other types of temperature rises. The material temperature-dependent constants are illustrated in Table 1.

2.2 Nonlocal strain gradient elasticity theory

According to the strain gradient elasticity theory, the total normal stress, σ_{xx}^t and shear stress, σ_{xz}^t components at any point are given by, Li and Hu (2016):

$$\begin{Bmatrix}\sigma_{xx}^t\\ \sigma_{xz}^t\end{Bmatrix} = \begin{Bmatrix}\sigma_{xx}^c\\ \sigma_{xz}^c\end{Bmatrix} - \begin{Bmatrix}\nabla\sigma_{xx}^h\\ \nabla\sigma_{xz}^h\end{Bmatrix} \tag{7}$$

where ∇ refers the one dimensional differential operator defined by $\nabla = \frac{\partial}{\partial x}$ Laplacian operator, while $\boldsymbol{\sigma_{xx}^c}$, σ_{xx}^h, $\boldsymbol{\sigma_{xz}^c}$ and σ_{xz}^h are the classical and higher-order normal and shear stress components; respectively which can be defined as, Al-shujairi and Mollamahmutoğlu (2018)

$$\begin{Bmatrix}\sigma_{xx}^c\\ \sigma_{xz}^c\end{Bmatrix} = \begin{Bmatrix}\int_\Omega E(z)\alpha_0(\boldsymbol{x'},\boldsymbol{x},e_0a)\varepsilon'_{xx}(\boldsymbol{x'})d\Omega\\ \int_\Omega G(z)\alpha_0(\boldsymbol{x'},\boldsymbol{x},e_0a)\gamma'_{xz}(\boldsymbol{x'})d\Omega\end{Bmatrix},$$
$$\begin{Bmatrix}\sigma_{xx}^h\\ \sigma_{xz}^h\end{Bmatrix} = \begin{Bmatrix}l_m^2\int_\Omega E(z)\alpha_1(\boldsymbol{x'},\boldsymbol{x},e_1a)\nabla\varepsilon'_{xx}(\boldsymbol{x'})d\Omega\\ l_m^2\int_\Omega G(z)\alpha_1(\boldsymbol{x'},\boldsymbol{x},e_1a)\nabla\gamma'_{xz}(\boldsymbol{x'})d\Omega\end{Bmatrix} \tag{8}$$

with ∇ refers to the one-dimensional differential operator, α_0 and α_1, respectively refer to the classical and higher-order nonlocal kernel functions, while e_0a and e_1a are the nonlocality coefficients (Eringen 1983) and l_m is the material length scale parameter. Assuming $e = e_0 = e_1$ and the nonlocal functions $\alpha_0(\boldsymbol{x'},\boldsymbol{x},e_0a)$ and $\alpha_1(\boldsymbol{x'},\boldsymbol{x},e_1a)$ are in the frame of the assumptions of (Eringen (1983), and using the linear differential operator, the nonlocal constitutive relations incorporating the thermal effect can be expressed as, Lim *et al*. (2015), Bensaid *et al*. (2018):

$$\left[1 - (ea)^2\frac{\partial^2}{\partial x^2}\right]\begin{Bmatrix}\sigma_{xx}^t\\ \sigma_{xz}^t\end{Bmatrix} = \left[1 - l_m^2\frac{\partial^2}{\partial x^2}\right]\begin{Bmatrix}E(z)\varepsilon_{xx}\\ G(z)\gamma_{xz}\end{Bmatrix} - \begin{Bmatrix}E(z)\alpha_{xx}\Delta T\\ 0\end{Bmatrix} \tag{9}$$

where ε_{xx} and γ_{xz} are the normal and shear strain components; respectively. α_{xx} and ΔT are respectively the thermal expansion coefficient and the temperature rise.

2.3 Kinematic and Kinetic relations

There are different types of beam and plate theories in the literature for the shear deformation effect. In this study, the Reddy's third-order shear deformation model (TSDT) is used. Based on Reddy's beam model, the displacement field is in the form, Najafi *et al*. (2017), Ebrahimi and Barati (2018), Le *et al*. (2020)

$$\begin{Bmatrix} u_x(x,z,t) \\ u_z(x,z,t) \end{Bmatrix} = \begin{bmatrix} 1 & g(z)\frac{\partial}{\partial x} & -f(z) \\ 0 & 1 & 0 \end{bmatrix} \begin{Bmatrix} u_0(x,t) \\ w_0(x,t) \\ \phi(x,t) \end{Bmatrix} \quad (10)$$
$$\text{and } u_y(x,z,t) = 0$$

Here, u_x, u_y and u_z denote the displacements in *x*, *y*, and *z* axes respectively, and $u_0(x,t)$ and $w_0(x,t)$ represent the mid-plane displacements in the axial and transverse directions, and $\phi(x,t)$ is the rotation of the cross-section, where $f(z)$ and $g(z)$ are given by Rahmani, and Jandaghian (2015)

$$\begin{Bmatrix} g(z) \\ f(z) \end{Bmatrix} = \begin{Bmatrix} -\beta z^3 \\ z(1-\beta z^2) \end{Bmatrix} \text{ and } \beta = \frac{4}{3h^2} \quad (11)$$

with *h* refers to beam height. According to the displacement field defined in Eqs. (10) and (11), the normal and shear strains are given by Rahmani and Jandaghian, (2015); Le *et al*. (2020):

$$\begin{Bmatrix} \varepsilon_{xx} \\ \gamma_{xz} \end{Bmatrix} = \begin{bmatrix} \frac{\partial}{\partial x} & 0 \\ \frac{\partial}{\partial z} & \frac{\partial}{\partial x} \end{bmatrix} \begin{Bmatrix} u_x(x,z,t) \\ u_z(x,z,t) \end{Bmatrix} + \begin{Bmatrix} \frac{1}{2}\left(\frac{\partial w_0}{\partial x}\right)^2 \\ 0 \end{Bmatrix} = \begin{Bmatrix} \varepsilon_{xx}^{(0)} + z\varepsilon_{xx}^{(1)} + z^3\varepsilon_{xx}^{(3)} \\ \gamma_{xz}^{(0)} + z^2\gamma_{xz}^{(2)} \end{Bmatrix} \quad (12a)$$

$$\varepsilon_{xx}^{(0)} = \frac{\partial u_0}{\partial x} + \frac{1}{2}\left(\frac{\partial w_0}{\partial x}\right)^2, \quad \varepsilon_{xx}^{(1)} = \frac{\partial \phi}{\partial x}, \quad \varepsilon_{xx}^{(3)} = -\beta\left(\frac{\partial \phi}{\partial x} + \frac{\partial^2 w_0}{\partial x^2}\right) \quad (12b)$$

$$\gamma_{xz}^{(0)} = \phi + \frac{\partial w_0}{\partial x}, \quad \gamma_{xz}^{(2)} = -\psi\left(\phi + \frac{\partial w_0}{\partial x}\right), \ \psi = \frac{4}{h^2} \quad (12c)$$

Constitutive relationships can be expressed as follows, Xie *et al*. (2020)

$$\begin{Bmatrix} \sigma_{xx} \\ \tau_{xz} \end{Bmatrix} = \begin{bmatrix} Q_{11}(z) & 0 \\ 0 & Q_{66}(z) \end{bmatrix} \begin{Bmatrix} \varepsilon_{xx} \\ \gamma_{xz} \end{Bmatrix} \quad \text{with} \quad Q_{11}(z) = \frac{E(z)}{1-\upsilon^2}, \ Q_{66}(z) = \frac{E(z)}{2(1+\upsilon)} \quad (13)$$

The resultant normal forces, bending moment, axial forces, and shear forces are expressed as, Ebrahimi and Barati (2016a, b)

$$\begin{Bmatrix} N \\ M \\ M_h \end{Bmatrix} = \int_A \begin{Bmatrix} 1 \\ z \\ f(z) \end{Bmatrix} \sigma_{xx}^t dA, \quad Q_h = \int_A \frac{df(z)}{dz} \tau_{xz}^t dA \quad (14)$$

and the higher-order stress resultants are given by, Al-shujairi and Mollamahmutoğlu (2018)

$$\begin{Bmatrix} N^h \\ M^h \\ M_h^h \end{Bmatrix} = \int_A \begin{Bmatrix} 1 \\ z \\ f(z) \end{Bmatrix} \sigma_{xx}^h dA, \quad Q_h^h = \int_A \frac{df(z)}{dz} \tau_{xz}^h dA \quad (15)$$

2.4 Thermal effect and thermomechanical relations

Considering the temperature effect due to the thermal environment, the forces, moments, and higher-order moments resultants due to thermal load rather than the axial direction can be neglected since the thickness and width are small compared to length of the beams. The resultant normal force and bending moment and higher-order moments due to the temperature field, N^T, M^T, and P^T are given by, Najafi *et al*. (2017)

$$\begin{Bmatrix} N^T \\ M^T \\ P^T \end{Bmatrix} = \begin{Bmatrix} \int_{-h/2}^{h/2} E(z,T)\alpha(z,T)\Delta T(z)dz \\ \int_{-h/2}^{h/2} zE(z,T)\alpha(z,T)\Delta T(z)dz \\ \int_{-h/2}^{h/2} z^3E(z,T)\alpha(z,T)\Delta T(z)dz \end{Bmatrix} \quad (16)$$

where $\alpha(z,T)$ and $\Delta T(z)$ respectively refer to the thermal expansion coefficient and the temperature change which can defined as, $\Delta T(z) = T(z) - T_0$, in which T0 is the reference value of material with zero thermal strain. Using Eqs. (10)-(16), the resultant forces are expressed as, Rahmani and Jandaghian, (2015)

$$\begin{Bmatrix} N \\ M \\ P \end{Bmatrix} = \begin{bmatrix} A_{11} & B_{11} & E_{11} \\ B_{11} & D_{11} & F_{11} \\ E_{11} & F_{11} & H_{11} \end{bmatrix} \begin{Bmatrix} \varepsilon_{xx}^{(0)} \\ \varepsilon_{xx}^{(1)} \\ \varepsilon_{xx}^{(3)} \end{Bmatrix} + \begin{Bmatrix} N^T \\ M^T \\ P^T \end{Bmatrix} \quad \text{and} \quad \begin{Bmatrix} \mathrm{Q} \\ \mathrm{R} \end{Bmatrix} = \begin{bmatrix} A_{55} & D_{55} \\ D_{55} & F_{55} \end{bmatrix} \begin{Bmatrix} \gamma_{xz}^{(0)} \\ \gamma_{xz}^{(2)} \end{Bmatrix} \quad (17)$$

with

$$[A_{11} \quad B_{11} \quad E_{11} \quad D_{11} \quad F_{11} \quad H_{11}] = \int_A Q_{11}(z)[1 \quad z \quad z^2 \quad z^3 \quad z^4 \quad z^6]dA$$
$$[A_{55} \quad D_{55} \quad F_{55}] = \int_A Q_{66}(z)[1 \quad z^2 \quad z^4]dA \quad (18)$$

2.5 Magnetic effect

Assume that the considered microbeam is exposed to the magnetic field. Maxwell's equations are employed to incorporate the magnetic field effect, (Arani and Jalaei 2017). Employing the Maxwell's equations, magnetic field vector (h) current density vector (J), magnetic field permeability (η), electric field vector (e), and magnetic field density (H) are described as, Esen *et al*. (2021b)

$$\mathrm{J} = \nabla \times \mathrm{h}, \quad \nabla \times \mathrm{e} = -\eta \frac{\partial \mathrm{h}}{\partial t}, \qquad \nabla \cdot \mathrm{h}=0 \quad (19)$$

$$\mathrm{e} = -\eta\left(\frac{\partial \mathrm{U}}{\partial t} \times \mathrm{H}\right), \ \mathrm{h}=\nabla \times (\mathrm{U} \times \mathrm{H}) \quad (20)$$

where, $\mathrm{U} = u\vec{\mathrm{i}} + v\vec{\mathrm{j}} + w\vec{\mathrm{k}}$, is the displacement field vector. Assuming longitudinal magnetic field affecting the microbeam is a vector, with $\mathrm{H} = H_x\vec{\mathrm{i}}$, the magnetic field is described by, Esen *et al*. (2021a), Sobhy and Zenkour (2018):

$$\mathrm{h} = -H_x\left(\frac{\partial v}{\partial y}+\frac{\partial w}{\partial z}\right)\vec{\mathrm{i}} + H_x\frac{\partial v}{\partial x}\vec{\mathrm{j}} + H_x\frac{\partial w}{\partial x}\vec{\mathrm{k}}. \tag{21}$$

Due to the magnetic field, the Lorentz force is given by:

$$f_m = f_{mx}\vec{\mathrm{i}} + f_{my}\vec{\mathrm{j}} + f_{mz}\vec{\mathrm{k}} = \eta(\mathrm{J}\times \mathrm{H}) = \eta\begin{bmatrix} 0\vec{\mathrm{i}} + H_x^2\left(\frac{\partial^2 v}{\partial x^2}+\frac{\partial^2 v}{\partial y^2}+\frac{\partial^2 w}{\partial y\partial z}\right)\vec{\mathrm{j}} \\ +H_x^2\left(\frac{\partial^2 w}{\partial x^2}+\frac{\partial^2 w}{\partial z^2}+\frac{\partial^2 v}{\partial y\partial z}\right)\vec{\mathrm{k}}\end{bmatrix} \tag{22}$$

Assuming that Lorentz force, f_m applies in the transverse z direction only, thus, Eq. (23) can be rewritten as

$$f_{mz} = \eta H_x^2\left(\frac{\partial^2 w}{\partial x^2}+\frac{\partial^2 w}{\partial z^2}+\frac{\partial^2 v}{\partial y\partial z}\right) \tag{23}$$

Using Eqs. (10) and (23), the Lorentz force is derived as:

$$F_{lz} = \eta h H_x^2\frac{\partial^2 u_z}{\partial x^2} = \eta h H_x^2\frac{\partial^2 w}{\partial x^2} \tag{24}$$

2.6 Dynamic equations of motion

Using Hamilton principle, Lin *et al*. (2020)

$$\int_{t1}^{t2}(\delta U_s + \delta U_{Th} - \delta T + \delta V)dt = 0 \tag{25}$$

with δU_s refers to the variation of strain energy which can be expressed as, Ebrahimi and Barati (2016), Al-shujairi and Mollamahmutoğlu (2018)

$$\delta U_s = \int_0^t\int_\Omega(\sigma_{xx}^c\delta\varepsilon_{xx}^c + \tau_{xz}^c\delta\gamma_{xz}^c + \sigma_{xx}^h\nabla\delta\varepsilon_{xx} + \tau_{xz}^h\nabla\delta\gamma_{xz})d\Omega\mathrm{d}t = \int_0^t\int_\Omega(\sigma_{xx}^t\delta\varepsilon_{xx} + \tau_{xz}^t\delta\gamma_{xz})d\Omega\mathrm{d}t + \int_0^t\left[\int_A(\sigma_{xx}^h\delta\varepsilon_{xx} + \tau_{xz}^h\delta\gamma_{xz})dA\right]_0^L dt \tag{26a}$$

$$\delta U_s = \int_0^l\left(N\frac{\partial\delta u_0}{\partial x} - M\frac{\partial^2\delta w_0}{\partial x^2} + M_h\left(\frac{\partial^2\delta w_0}{\partial x^2} - \frac{\partial\delta\phi}{\partial x}\right) + Q_h\left(\frac{\partial\delta w_0}{\partial x} - \delta\phi\right)\right)\mathrm{d}x + \left[\int_A\left(N^h\frac{\partial\delta u_0}{\partial x} - M^h\frac{\partial^2\delta w_0}{\partial x^2} + M_h^h\left(\frac{\partial^2\delta w_0}{\partial x^2} - \frac{\partial\delta\phi}{\partial x}\right) + Q_h^h\left(\frac{\partial\delta w_0}{\partial x} - \delta\phi\right)\right)\right]_0^L \tag{26b}$$

δU_{Th} refers to the variation of strain energy due to thermal effect which can be expressed as, Al-shujairi and Mollamahmutoğlu (2018)

$$\delta U_{Th} = -\int_0^l\left(C(z)\Delta T\frac{\partial w_0}{\partial x}\frac{\partial\delta w_0}{\partial x}\right)dx, \quad C(z) = \int_A\frac{E(z)}{1-2\nu}\alpha(z)dA \tag{26c}$$

with ΔT is the temperature rise and α(z) refers the effective thermal expansion coefficient. On the other hand, the variation of the total kinetic energy which δT can be given by

$$\delta T = \int_0^l\int_A\rho(z)[(\dot{u}_x\delta\dot{u}_x + \dot{u}_z\delta\dot{u}_z)]\,dAdx = \int_0^l\Big[I_0\left(\frac{\partial u_0}{\partial t}\frac{\partial\delta u_0}{\partial t} + \frac{\partial w_0}{\partial t}\frac{\partial\delta w_0}{\partial t}\right) - I_1\left(\frac{\partial u_0}{\partial t}\frac{\partial^2\delta w_0}{\partial x\partial t} + \frac{\partial^2 w_0}{\partial x\partial t}\frac{\partial\delta u_0}{\partial t}\right) + I_3\left(\frac{\partial^2 w_0}{\partial x\partial t}\frac{\partial^2\delta w_0}{\partial x\partial t}\right) + I_2\left\{\frac{\partial u_0}{\partial t}\left(\frac{\partial^2\delta w_0}{\partial x\partial t} - \frac{\partial\delta\phi}{\partial t}\right) + \frac{\partial\delta u_0}{\partial t}\left(\frac{\partial^2 w_0}{\partial x\partial t} - \frac{\partial\phi}{\partial t}\right)\right\} - I_4\left\{\frac{\partial^2 w_0}{\partial x\partial t}\left(\frac{\partial^2\delta w_0}{\partial x\partial t} - \frac{\partial\delta\phi}{\partial t}\right) + \frac{\partial^2\delta w_0}{\partial x\partial t}\left(\frac{\partial^2 w_0}{\partial x\partial t} - \frac{\partial\phi}{\partial t}\right)\right\} + I_5\left(\frac{\partial^2 w_0}{\partial x\partial t} - \frac{\partial\phi}{\partial t}\right)\left(\frac{\partial^2\delta w_0}{\partial x\partial t} - \frac{\partial\delta\phi}{\partial t}\right)\Big]dx \tag{27}$$

With the inertia coefficients, Xie *et al*. (2020);

$$(I_0, I_1, I_2, I_3, I_4, I_5) = \int_A\rho(z)\times(1, z, f(z), z^2, zf(z), (f(z))^2)dA \tag{28}$$

The variation of the work done by applied external mechanical and magnetic loads is expressed in the following form:

$$\delta V = \int_0^l\left(P_x\left[\frac{\partial\delta u_0}{\partial x} + \frac{\partial w_0}{\partial x}\frac{\partial\delta w_0}{\partial x}\right] + q\delta w_0 + f\delta u_0\right)dx + \int_0^l\left(\eta h H_x^2\frac{\partial^2 w_0}{\partial x^2}\right)w_0(x,t)\delta w_0 dx \tag{29}$$

where P_x is the applied axial buckling load and q and f are respectively the transverse and axial distributed loads per unit length. Additionally, if the nanobeam is subjected to a moving point load $q(t)$, the potential of the moving load is given by, (Nguyen *et al*. 2017)

$$\delta V_{q(t)} = \int_0^l q(t)\delta w_0(x,t)\delta(x_P - vt)dx \tag{30}$$

where δ(.) is the Dirac delta function, and x is the abscissa, measured from the left end of the beam. Applying the Hamilton's principle and evaluating the integral and setting each coefficient of δu_0, δw_0 and $\delta\phi$ to zero, the equations of motion based on the third order higher-order shear deformation beam theory are:

$$\begin{gathered}\frac{\partial N}{\partial x} + f = I_0\frac{\partial^2 u_0}{\partial t^2} + (I_1 - I_2)\frac{\partial^3 w_0}{\partial x\partial t^2} - I_2\frac{\partial^2\phi}{\partial t^2} \\ \frac{\partial^2 M}{\partial x^2} - \frac{\partial^2 M_h}{\partial x^2} + \frac{\partial Q_h}{\partial x} + q\delta(x_P - vt) - (P_x + C(z) + \eta h H_x^2)\frac{\partial^2 w_0}{\partial x^2} = I_0\frac{\partial^2 u_0}{\partial t^2} + (I_1 - I_2)\frac{\partial^3 u_0}{\partial x\partial t^2} - (I_5 - 2I_4 + I_3)\frac{\partial^4 w_0}{\partial x^2\partial t^2} + (I_4 - I_5)\frac{\partial^3\phi}{\partial x\partial t^2} \\ Q_h - \frac{\partial M_h}{\partial x} = -I_2\frac{\partial^2 u_0}{\partial t^2} + (I_4 - I_5)\frac{\partial^3 w_0}{\partial x\partial t^2} + I_5\frac{\partial^2\phi}{\partial t^2}\end{gathered} \tag{31}$$

To write the differential equations of motion in terms of displacements, the following relations for the stress resultants in terms of displacements are obtained by substituting from Eqs (10), (12), (14), and (15) into Eq. (6) results

$$\begin{gathered}\left(1 - (ea)^2\frac{\partial^2}{\partial x^2}\right)N = \left(1 - l_m^2\frac{\partial^2}{\partial x^2}\right)\left(A_0\frac{\partial u_0}{\partial x} + (A_2 - A_1)\frac{\partial^2 w_0}{\partial x^2} - A_2\frac{\partial\phi}{\partial x}\right) \\ \left(1 - (ea)^2\frac{\partial^2}{\partial x^2}\right)M = \left(1 - l_m^2\frac{\partial^2}{\partial x^2}\right)\left(A_0\frac{\partial u_0}{\partial x} + (A_4 - A_3)\frac{\partial^2 w_0}{\partial x^2} - A_4\frac{\partial\phi}{\partial x}\right) \\ \left(1 - (ea)^2\frac{\partial^2}{\partial x^2}\right)Q_h = G_0\left(1 - l_m^2\frac{\partial^2}{\partial x^2}\right)\left(\frac{\partial w_0}{\partial x} - \phi\right) \\ \left(1 - (ea)^2\frac{\partial^2}{\partial x^2}\right)M_h = \left(1 - l_m^2\frac{\partial^2}{\partial x^2}\right)\left(A_2\frac{\partial u_0}{\partial x} - (A_5 - A_4)\frac{\partial^2 w_0}{\partial x^2} - A_5\frac{\partial\phi}{\partial x}\right)\end{gathered} \tag{32a}$$

with

$$[A_0 \quad A_1 \quad A_2 \quad A_3 \quad A_4 \quad A_5] \tag{32b}$$

$$= \int_A Q_{11}(z)[1 \quad z \quad f(z) \quad z^2 \quad zf(z) \quad (f(z))^2]dA$$

$$G_0 = \int_A Q_{66}(z)\left(\frac{df(z)}{dz}\right)^2 dA$$

Eq. (33a) can be expressed in terms of the displacement field as:

$$N = (ea)^2\left(I_0\frac{\partial^3 u_0}{\partial x\partial t^2} + (I_1 - I_2)\frac{\partial^4 w_0}{\partial x^2\partial t^2} - I_2\frac{\partial^3\phi}{\partial x\partial t^2} - \frac{\partial f}{\partial x}\right) + \left(1 - l_m^2\frac{\partial^2}{\partial x^2}\right)\left(A_0\frac{\partial u_0}{\partial x} + (A_2 - A_1)\frac{\partial^2 w_0}{\partial x^2} - A_2\frac{\partial\phi}{\partial x}\right)$$

$$M = (ea)^2\begin{pmatrix} I_0\frac{\partial^2 w_0}{\partial t^2} + I_1\frac{\partial^3 u_0}{\partial x\partial t^2} + (I_4 - I_3)\frac{\partial^4 w_0}{\partial x^2\partial t^2} - I_4\frac{\partial^3\phi}{\partial x\partial t^2} \\ -q\delta(x_P - vt) + (P_x + C(z)\Delta T)\frac{\partial^2 w_0}{\partial x^2}\end{pmatrix} + \left(1 - l_m^2\frac{\partial^2}{\partial x^2}\right)\left(A_0\frac{\partial u_0}{\partial x} + (A_4 - A_3)\frac{\partial^2 w_0}{\partial x^2} - A_4\frac{\partial\phi}{\partial x}\right) \quad (32c)$$

$$Q_h = (ea)^2\left(-I_2\frac{\partial^4 u_0}{\partial x^2\partial t^2} - (I_5 - I_4)\frac{\partial^5 w_0}{\partial x^3\partial t^2} + I_5\frac{\partial^4\phi}{\partial x^2\partial t^2}\right) + \left(1 - l_m^2\frac{\partial^2}{\partial x^2}\right)\begin{pmatrix} A_2\frac{\partial^2 u_0}{\partial x^2} - (A_5 - A_4)\frac{\partial^3 w_0}{\partial x^3} + \\ A_5\frac{\partial^2\phi}{\partial x^2} + G_0\left(\frac{\partial w_0}{\partial x} - \phi\right)\end{pmatrix}$$

Substitute Eqs. (32c) into Eqs. (31), the following differential equations of motion in terms of displacement field are obtained:

$$\left(1 - (ea)^2\frac{\partial^2}{\partial x^2}\right)\begin{pmatrix} -I_0\frac{\partial^2 u_0}{\partial t^2} + (I_1 - I_2)\frac{\partial^3 w_0}{\partial x\partial t^2} \\ +I_2\frac{\partial^2\phi}{\partial t^2} + f\end{pmatrix} + \left(1 - l_m^2\frac{\partial^2}{\partial x^2}\right)\begin{pmatrix} A_0\frac{\partial^2 u_0}{\partial x^2} + (A_2 - A_1)\frac{\partial^3 w_0}{\partial x^3} \\ -A_2\frac{\partial^2\phi}{\partial x^2}\end{pmatrix} = 0$$

$$\left(1 - (ea)^2\frac{\partial^2}{\partial x^2}\right)\begin{pmatrix} -I_0\frac{\partial^2 w_0}{\partial t^2} - I_1\frac{\partial^3 u_0}{\partial x\partial t^2} - (I_4 - I_3)\frac{\partial^4 w_0}{\partial x^2\partial t^2} \\ +I_4\frac{\partial^3\phi}{\partial x\partial t^2} + q\delta(x_P - vt) \\ -(P_x + C(z)\Delta T + \eta hH_x^2)\frac{\partial^2 w_0}{\partial x^2}\end{pmatrix} + \left(1 - l_m^2\frac{\partial^2}{\partial x^2}\right)\left(A_1\frac{\partial^3 u_0}{\partial x^3} + (A_4 - A_3)\frac{\partial^4 w_0}{\partial x^4} - A_4\frac{\partial^3\phi}{\partial x^3}\right) = 0 \quad (33)$$

$$\left(1 - (ea)^2\frac{\partial^2}{\partial x^2}\right)\left(I_2\frac{\partial^2 u_0}{\partial t^2} + (I_5 - I_4)\frac{\partial^3 w_0}{\partial x\partial t^2} - I_5\frac{\partial^2\phi}{\partial t^2}\right) + \left(1 - l_m^2\frac{\partial^2}{\partial x^2}\right)\begin{pmatrix} -A_2\frac{\partial^2 u_0}{\partial x^2} - (A_5 - A_4)\frac{\partial^3 w_0}{\partial x^3} + \\ A_5\frac{\partial^2\phi}{\partial x^2} + G_0\left(\frac{\partial w_0}{\partial x} - \phi\right)\end{pmatrix} = 0$$

Moreover, the corresponding boundary conditions at $x = 0$ and $x = L$ as follows:

$$\delta u_0(N) = 0 \Rightarrow N = 0 \text{ or } u_0 = 0 \quad \& \quad \frac{\partial\delta u_0}{\partial x}(N^h) = 0 \Rightarrow N^h = 0 \text{ or } \frac{\partial u_0}{\partial x} = 0$$

$$\delta w_0\left(\frac{\partial M}{\partial x} - \frac{\partial M_h}{\partial x} + Q_h + (P_x + C(z)\Delta T)\frac{\partial w_0}{\partial x}\right) = 0$$

$$\Rightarrow \frac{\partial M}{\partial x} - \frac{\partial M_h}{\partial x} + Q_h + (P_x + C(z)\Delta T)\frac{\partial w_0}{\partial x} = 0 \text{ or } w_0 = 0$$

$$\frac{\partial\delta w_0}{\partial x}(M) = 0 \Rightarrow \frac{\partial w_0}{\partial x} = 0 \text{ or } M = 0 \ \& \ \frac{\partial^2\delta w_0}{\partial x^2}(M^h) = 0 \quad (34)$$

$$\Rightarrow \frac{\partial^2 w_0}{\partial x^2} = 0 \text{ or } M^h = 0$$

$$\delta\left(\frac{\partial^2 w_0}{\partial x^2} - \frac{\partial\phi}{\partial x}\right)(M^h) = 0 \Rightarrow \frac{\partial^2 w_0}{\partial x^2} - \frac{\partial\phi}{\partial x} = 0 \text{ or } M^h = 0 \ \& \ \delta\left(\frac{\partial w_0}{\partial x} - \phi\right)(Q^h + M_h) = 0 \Rightarrow \frac{\partial w_0}{\partial x} - \phi = 0 \text{ or } Q^h + M_h = 0$$

3. Analytical solution methodology

Consider a simply supported beam subjected to a moving point load. In addition to the mechanical moving load, the beam is exposed to magnetic field and uniform temperature rise of ΔT. Navier's approach will be employed to obtain the natural frequency of the free vibration response and the transient displacement time response of forced vibration under moving point load. For the simply supported boundary conditions, For the classical boundary conditions in Eq. (34) (at $x = 0$ and $x = L$)

$$N = 0,\ w_0 = 0,\ M = 0 \quad (35)$$

And for non-classical boundary conditions (at $x = 0$ and $x = L$)

$$\frac{\partial u_0}{\partial x} = 0, \qquad Q_{xz}^h = 0, \qquad \frac{\partial\phi}{\partial x} = 0 \quad (36)$$

Assuming the vibration solution is periodic in time, the displacements are in the following form:

$$\begin{Bmatrix} u_0(x,t) \\ w_0(x,t) \\ \phi_0(x,t)\end{Bmatrix} = \sum_n \begin{Bmatrix} U_n\cos\beta x\, e^{i\omega_n t} \\ W_n\sin\beta x\, e^{i\omega_n t} \\ \Phi_n\cos\beta x\, e^{i\omega_n t}\end{Bmatrix},\ \beta = \left(\frac{n\pi}{L}\right) \quad (37)$$

where $i = \sqrt{-1}$, and ω_n is the natural vibration frequencies. For any U_n, W_n, and Φ_n the series solution (37), the spatial dependent trigonometric orthogonal functions satisfy the kinematic boundary conditions.

$$\sum_{n=1}^{N}[[\boldsymbol{K}] - \omega_n^2[\boldsymbol{M}]]\begin{Bmatrix} U_n \\ W_n \\ \Phi_n\end{Bmatrix} = \begin{Bmatrix} 0 \\ -q \\ 0\end{Bmatrix} \quad (38)$$

Neglecting the effect of external force, the following Eigenvalue equation is derived.

$$[\mathbf{K} - \omega_n^2\mathbf{M}]\{\mathbf{d}\} = \{0\} \quad (39a)$$

Here, $\{\mathbf{d}\} = [U_n \quad W_n \quad \Phi_n]^{\boldsymbol{T}}$ are the unknowns to be determined $\mathbf{K}$ and $\mathbf{M}$ are stiffness and mass matrices, respectively. These matrices are described as follows:

$$\mathbf{K} = c_2\begin{bmatrix} A_0\beta^2 & (A_2 - A_1)\beta^3 & A_2\beta^2 \\ -A_1\beta^3 & (A_3 - A_4)\beta^4 + c_1\beta^2\begin{pmatrix} P_x \\ +C(z)\Delta T \\ +\eta hH_x^2\end{pmatrix} & A_4\beta^3 \\ -A_2\beta^2 & -((A_5 - A_4)\beta^3 + G_0\beta) & (A_5\beta^2 + G_0)\end{bmatrix} \quad (39b)$$

$$\mathbf{M} = c_1\begin{bmatrix} I_0 & -\beta(I_1 - I_2) & -I_2 \\ -I_1\beta & I_0 - \beta^2(I_4 - I_3) & I_4\beta \\ -I_2 & -(I_5 - I_4)\beta & I_5\end{bmatrix} \quad (39c)$$

$$c_1 = 1 + (ea)^2\beta^2,\ c_2 = 1 + l_m^2\beta^2 \quad (39d)$$

For the forced vibration response of the FG Reddy nanobeam, substituting Eq. (37) into (33) one can derive the following equation:

$$\mathbf{M}\ddot{\mathbf{d}} + \mathbf{K}\,\mathbf{d} = \mathbf{q} \quad (40)$$

where $\mathbf{q}$ is the external force vector and it can be defined according to the type of the transverse load $q(x)$ as given

Table 2 Comparison of the first frequency parameter (λ_1) for the simply supported FGM beam with Al2O3 and Al

Power-law exponent *k*	Fundamental frequency, λ_1			
	Refs.	*L/h* = 10	*L/h* = 30	*L/h* = 100
0	Present	2.8028	2.8436	2.8485
	Nguyen *et al*. (2013)	2.7970	2.8430	2.8480
	Sina *et al*. (2009)	2.8026	2.8438	2.8486
	Esen (2019)	2.8027	2.8458	2.8488
0.3	Present	2.6993	2.7367	2.7418
	Nguyen *et al*. (2013)	2.6950	2.7370	2.7420
	Sina *et al*. (2009)	2.6992	2.7368	2.7412
	Esen (2019)	2.6953	2.7361	2.7421

Table 3 Comparison of the maximum mid-span responses to a load moving at constant velocities, for FGM beams.

Source	SUS304 (132 m/s)	*k* = 0.2 (222 m/s)	*k* = 0.5 (198 m/s)	*k* = 1 (179 m/s)	*k* = 2 (164 m/s)	*k* = 5 (164 m/s)	Al2O3 (252m/s)
Present	**1.7316**	**1.0336**	**1.1435**	**1.2690**	**1.3365**	**1.6314**	**0.9326**
Şimşek and Kocatürk (2009)	1.7324	1.0344	1.1444	1.2503	1.3376	-	0.9328
Khalili *et al*. (2010)	1.7301	1.0333	1.1429	1.2486	1.3359	-	0.9317

below, Reddy (2007):

$$\mathbf{q} = \begin{Bmatrix} 0 \\ Q_n c_1 \\ 0 \end{Bmatrix} \tag{41}$$

The external load can be expanded in Fourier series and the term Q_n is defined as follows:

$$q(x) = \sum_n Q_n \sin\frac{n\pi x}{L} \quad \text{with}$$
$$Q_n = \frac{2}{L}\int_0^L q(x)\sin\frac{n\pi x}{L}dx \tag{42a}$$

For point load at x_p, the external load is defined as $q(x) = q_0\delta(x - x_p)$, and Q_n is derived as:

$$Q_n = \frac{2F}{L}\sin\left(\frac{n\pi}{L}\right)x_p, n = 1, 2, 3, \ldots$$
$$x_p = \frac{L}{2}; \quad \xrightarrow{yields} Q_n = \frac{2F}{L}\sin\frac{n\pi}{2}, n = 1, 2, 3, \ldots \tag{42b}$$

For uniform load

$$q(x) = q_0,\ Q_n = \frac{4q_0}{n\pi}, n = 1, 3, 5, \ldots \tag{43}$$

4. Model verification

To check and verify the accuracy of the developed procedure to investigate the dynamic behaviour of functionally graded beams, consider a simply supported functionally graded beam made of aluminium and Alumina, and the following material properties are used: Alumina (ceramic): E_c = 380 GPa; ρ_c = 3800 kg/m^3; υ_c = 0.23. Aluminum (metal): E_m = 70 GPa; ρ_m = 2700 kg/m^3; υ_m = 0.23

4.1 Verification of free vibration

The developed numerical procedure is applied to obtain the fundamental frequency. The normalized frequency parameter, λ_1 defined as

$$\lambda_1 = \left(\frac{\omega_1 L^2}{h}\right)\sqrt{\left[\frac{\int_{-\frac{h}{2}}^{\frac{h}{2}}\rho(z)dz}{\int_{-\frac{h}{2}}^{\frac{h}{2}}E(z)dz}\right]} \tag{44}$$

The same problem was previously analyzed by Nguyen *et al*. (2013), Sina *et al*. (2009), and Esen (2019) for the same material properties and geometric parameters. The developed procedure is applied to detect the normalized fundamental frequency for different values of graduation index, *k*, and beam aspect ratio, (*L*/*h*). Comparing results obtained by the developed procedure and those obtained in literature, it may be observed that good agreement is obtained as depicted in Tables 2 and 3.

5. Numerical

The applicability of the developed procedure to study and analyze the thermomagnetic dynamic behavior of functionally graded nanosized beam structures under moving load is to be demonstrated in this section. Consider a simply supported functionally graded Reddy beam having he following material and geometrical characteristics: E_m = 70 GPa, ρ_m = 2700 kg/m^3, υ_m = 0.3, E_c = 380, $G_m = \frac{E_m}{2(1+\upsilon_m)}$ GPa, ρ_c = 3960 kg/m^3, υ_c = 0.3, $G_c = \frac{E_c}{2(1+\upsilon_c)}$, L = 10^{-9} m, beam aspect ratio, $\frac{L}{h} = 10$ otherwise stated. Both free and forced vibration behaviours are investigated. Effects of functionally graded material distribution, nonclassical parameters, magnetic field, as well as temperature variation are investigated and discussed.

5.1 Free vibration analysis

To investigate the effect of the FGM properties

Table 4 Comparisons of dimensionless frequencies of MCM FGM nanobeams for k and *L*/*h*, nonlocal and size parameters: $e_0a = l_m = 0$. Temperature increase and dimensionless magnetic field $\Delta T = H_x^m = 0$

		λ_1			λ_2			λ_3	
k	*L*/*h* = 10	*L*/*h* = 30	*L*/*h* = 100	*L*/*h* = 10	*L*/*h* = 30	*L*/*h* = 100	*L*/*h* = 10	*L*/*h* = 30	*L*/*h* = 100
0	9.7058	9.8510	9.8671	37.0738	39.1822	39.4520	78.0639	87.3526	88.6875
0.1	9.5609	9.7009	9.7189	36.5516	38.5905	38.8495	77.0529	86.0490	87.3413
0.3	9.3799	9.5143	9.5307	35.8929	37.8526	38.1022	75.7612	84.4194	85.6578
0.7	9.2235	9.3542	9.3678	35.3161	37.2175	37.4597	74.6084	83.0126	84.2137
1	9.1829	9.3127	9.3301	35.1626	37.0526	37.2918	74.2937	82.6464	83.8414
2	9.1843	9.3148	9.3317	35.1604	37.0601	37.3051	74.2719	82.6586	83.8627
5	9.3269	9.4609	9.4734	35.6878	37.6394	37.8864	75.3337	83.9422	85.1812
10	9.4616	9.5982	9.6162	36.1948	38.1848	38.4425	76.3761	85.1544	86.4143

Table 5 Comparisons of dimensionless frequencies of CMC FGM nanobeams for k and *L*/*h*, nonlocal and size parameters: $e_0a = l_m = 0$. Temperature increase and dimensionless magnetic field $\Delta T = H_x^m = 0$

		λ_1			λ_2			λ_3	
k	*L*/*h* = 10	*L*/*h* = 30	*L*/*h* = 100	*L*/*h* = 10	*L*/*h* = 30	*L*/*h* = 100	*L*/*h* = 10	*L*/*h* = 30	*L*/*h* = 100
0	9.7111	9.8513	9.8679	37.1466	39.1917	39.4524	78.3602	87.4006	88.6944
0.1	9.8134	9.9557	9.9741	37.5321	39.6056	39.8707	79.1498	88.3214	89.6330
0.3	9.9650	10.1112	10.1280	38.0919	40.2214	40.4906	80.2675	89.6852	91.0302
0.7	10.1391	10.2910	10.3086	38.7198	40.9322	41.2175	81.4812	91.2524	92.6513
1	10.2070	10.3618	10.3800	38.9591	41.2110	41.4972	81.9284	91.8638	93.2903
2	10.2761	10.4348	10.4562	39.1894	41.4973	41.7897	82.3235	92.4854	93.9486
5	10.1885	10.3467	10.3637	38.8477	41.1459	41.4397	81.5927	91.6974	93.1578
10	10.0446	10.1994	10.2178	38.3155	40.5613	40.8515	80.5256	90.4023	91.8284

Table 6 Comparisons of dimensionless frequencies of SIGMOID FGM nanobeams for k and *L*/*h*, nonlocal and size parameters: $e_0a = l_m = 0$. Temperature increase and dimensionless magnetic field $\Delta T = H_x^m = 0$

		λ_1			λ_2			λ_3	
k	*L*/*h* = 10	*L*/*h* = 30	*L*/*h* = 100	*L*/*h* = 10	*L*/*h* = 30	*L*/*h* = 100	*L*/*h* = 10	*L*/*h* = 30	*L*/*h* = 100
0	9.70997	9.85157	9.86799	37.14474	39.19514	39.45338	54.43583	87.43498	88.70539
0.1	9.70893	9.85155	9.86797	37.14031	39.19511	39.45330	54.41754	87.43486	88.70517
0.3	9.70364	9.85149	9.86785	37.11781	39.19500	39.45287	54.32517	87.43430	88.70404
0.7	9.69173	9.85134	9.86759	37.06683	39.19472	39.45190	54.11906	87.43297	88.70143
1	9.68462	9.85124	9.86743	37.03624	39.19453	39.45132	53.99749	87.43212	88.69987
2	9.67069	9.85104	9.86710	36.97600	39.19414	39.45015	53.76262	87.43036	88.69675
5	9.65903	9.85086	9.86683	36.92525	39.19378	39.44916	53.56925	87.42878	88.69409
10	9.65562	9.85080	9.86675	36.91032	39.19367	39.44886	53.51314	87.42829	88.69330

Table 7 Comparisons of dimensionless frequencies of MCM FGM nanobeams for k and *L*/*h*, nonlocal and size parameters: $e_0a = 1nm^2, l_m = 0$. Temperature increase and dimensionless magnetic field $\Delta T = H_x^m = 0$

		λ_1			λ_2			λ_3	
k	*L*/*h* = 10	*L*/*h* = 30	*L*/*h* = 100	*L*/*h* = 10	*L*/*h* = 30	*L*/*h* = 100	*L*/*h* = 10	*L*/*h* = 30	*L*/*h* = 100
0	9.2596	9.3979	9.4147	31.3916	33.1769	33.4042	56.8093	63.5688	64.5403
0.1	9.1214	9.2550	9.2709	30.9494	32.6759	32.8963	56.0735	62.6201	63.5596
0.3	8.9487	9.0770	9.0947	30.3917	32.0509	32.2603	55.1335	61.4344	62.3355
0.7	8.7995	8.9243	8.9372	29.9033	31.5132	31.7183	54.2945	60.4107	61.2837
1	8.7607	8.8846	8.8992	29.7733	31.3737	31.5762	54.0655	60.1439	61.0154
2	8.7620	8.8866	8.9045	29.7714	31.3798	31.5856	54.0497	60.1529	61.0292
5	8.8981	9.0259	9.0395	30.2180	31.8706	32.0797	54.8224	61.0870	61.9902
10	9.0266	9.1570	9.1741	30.6473	32.3322	32.5489	55.5810	61.9694	62.8860

Table 8 Comparisons of dimensionless frequencies of CMC FGM nanobeams for k and *L*/*h*, nonlocal and size parameters: $e_0a = 1nm^2, l_m = 0$. Temperature increase and dimensionless magnetic field $\Delta T = H_x^m = 0$

	λ_1			λ_2			λ_3		
k	*L*/*h* = 10	*L*/*h* = 30	*L*/*h* = 100	*L*/*h* = 10	*L*/*h* = 30	*L*/*h* = 100	*L*/*h* = 10	*L*/*h* = 30	*L*/*h* = 100
0	9.2647	9.3984	9.4127	31.4532	33.1849	33.4057	57.0248	63.6037	64.5453
0.1	9.3623	9.4981	9.5140	31.7796	33.5356	33.7599	57.5995	64.2739	65.2284
0.3	9.5068	9.6461	9.6624	32.2537	34.0567	34.2863	58.4128	65.2663	66.2451
0.7	9.6730	9.8177	9.8330	32.7854	34.6588	34.8985	59.2960	66.4067	67.4264
1	9.7378	9.8854	9.9028	32.9880	34.8948	35.1370	59.6215	66.8518	67.8899
2	9.8037	9.9553	9.9755	33.1829	35.1372	35.3884	59.9090	67.3042	68.3723
5	9.7202	9.8710	9.8893	32.8937	34.8397	35.0894	59.3772	66.7304	67.7934
10	9.5829	9.7304	9.7469	32.4430	34.3448	34.5914	58.6006	65.7882	66.8260

Table 9 Comparisons of dimensionless frequencies of SIGMOID FGM nanobeams for k and *L*/*h*, nonlocal and size parameters: $e_0a = 1nm^2, l_m = 0$. Temperature increase and dimensionless magnetic field $\Delta T = H_x^m = 0$

	λ_1			λ_2			λ_3		
k	*L*/*h* = 10	*L*/*h* = 30	*L*/*h* = 100	*L*/*h* = 10	*L*/*h* = 30	*L*/*h* = 100	*L*/*h* = 10	*L*/*h* = 30	*L*/*h* = 100
0	9.25710	9.39309	9.40874	35.41190	37.37107	37.61724	51.88509	83.36587	84.57707
0.1	9.25206	9.39303	9.40863	35.39044	37.37096	37.61684	51.79702	83.36533	84.57598
0.3	9.24070	9.39288	9.40837	35.34183	37.37070	37.61591	51.60050	83.36406	84.57349
0.7	9.23392	9.39279	9.40822	35.31267	37.37052	37.61536	51.48459	83.36325	84.57201
1	9.22064	9.39260	9.40791	35.25524	37.37015	37.61424	51.26064	83.36158	84.56903
2	9.20953	9.39242	9.40765	35.20685	37.36980	37.61329	51.07628	83.36007	84.56650
5	9.20627	9.39237	9.40758	35.19261	37.36969	37.61301	51.02277	83.35961	84.56575
10	9.25809	9.39310	9.40876	35.41612	37.37110	37.61732	51.90253	83.36598	84.57727

Table 10 Comparisons of dimensionless frequencies of MCM FGM nanobeams for k and *L*/*h*, nonlocal and size parameters:$e_0a = 0, l_m = 1nm^2$. Temperature increase and dimensionless magnetic field $\Delta T = H_x^m = 0$

	λ_1			λ_2			λ_3		
k	*L*/*h* = 10	*L*/*h* = 30	*L*/*h* = 100	*L*/*h* = 10	*L*/*h* = 30	*L*/*h* = 100	*L*/*h* = 10	*L*/*h* = 30	*L*/*h* = 100
0	10.1735	10.3251	10.3427	43.7845	46.2748	46.5916	107.2709	120.0348	121.8782
0.1	10.021	10.1687	10.1884	43.1678	45.5758	45.8824	105.8816	118.2432	120.0186
0.3	9.8319	9.9728	9.9894	42.3898	44.7044	45.0007	104.1066	116.0040	117.7090
0.7	9.6680	9.8047	9.8219	41.7086	43.9540	44.2391	102.5225	114.0705	115.7246
1	9.6254	9.7611	9.7769	41.5274	43.7595	44.0460	102.0900	113.5678	115.2147
2	9.6268	9.7635	9.7805	41.5247	43.7682	44.0516	102.0601	113.5844	115.2384
5	9.7763	9.9170	9.9359	42.1476	44.4529	44.7439	103.5192	115.3482	117.0547
10	9.9175	10.0608	10.077	42.7464	45.0967	45.3989	104.9517	117.0140	118.7476

distribution throughout the nanobeam thickness, the nondimensional natural frequencies of the 1st three vibration modes are detected using the developed procedure for nanobeams made of symmetric metal-ceramic-metal (MCM), symmetric ceramic-metal-ceramic (CMC), and Sigmoid FGM.

5.1.1 Effect of the nonclassical parameters

The dependency of the classical nondimensional natural frequencies on the material graduation parameter for MCM, CMC, and Sigmoid material distributions is respectively illustrated in Tables 4-6. It may be noticed that for symmetric metal-ceramic-metal (MCM) FGM beams graduating the FGM between 0 and 1 (0 < k < 1) decreases the classical nondimensional frequency parameter for all vibration modes at all values of beam aspect ratios. On the other hand, the nondimensional frequency parameter increases with increasing k for k > 1 due to increasing beam stiffness. The absolute relative percentage change in the nondimensional frequency parameter between k = 0 and k = 1 can be expressed as $\%\Delta\lambda_{i(k=0\rightarrow k=1)} = \left|\frac{\lambda_{i(k=0)}-\lambda_{i(k=1)}}{\lambda_{i(k=1)}}\right| \times 100$. This percentage change reaches about 5.7%. while the smaller values of this absolute relative percentage change between k = 1 and t k = 10, $\%\Delta\lambda_{i(k=1\rightarrow k=10)} = \left|\frac{\lambda_{i(k=10)}-\lambda_{i(k=1)}}{\lambda_{i(k=1)}}\right| \times 100$. It reaches about 3%. Additionally, it

Table 11 Comparisons of dimensionless frequencies of CMC FGM nanobeams for k and *L*/*h*, nonlocal and size parameters:$e_0a = 0, l_m = 1nm^2$. Temperature increase and dimensionless magnetic field $\Delta T = H_x^m = 0$

	λ_1			λ_2			λ_3		
k	*L*/*h* = 10	*L*/*h* = 30	*L*/*h* = 100	*L*/*h* = 10	*L*/*h* = 30	*L*/*h* = 100	*L*/*h* = 10	*L*/*h* = 30	*L*/*h* = 100
0	10.1791	10.3259	10.3421	43.8705	46.2862	46.5934	107.6780	120.1007	121.8787
0.1	10.2863	10.4354	10.4524	44.3258	46.7749	47.0873	108.7631	121.3660	123.1655
0.3	10.4452	10.5983	10.6143	44.9869	47.5020	47.8209	110.2989	123.2400	125.0866
0.7	10.6277	10.7871	10.8061	45.7285	48.3414	48.6741	111.9666	125.3934	127.3200
1	10.6989	10.8612	10.8802	46.0111	48.6708	49.0123	112.5812	126.2333	128.1934
2	10.7713	10.9376	10.9581	46.2831	49.0094	49.3561	113.1241	127.0881	129.0968
5	10.6795	10.8456	10.8638	45.8795	48.5940	48.9388	112.1200	126.0051	128.0101
10	10.5287	10.6911	10.7096	45.2510	47.9035	48.2392	110.6536	124.2255	126.1826

Table 12 Comparisons of dimensionless frequencies of SIGMOID FGM nanobeams for *k* and *L*/*h*, nonlocal and size parameters:$e_0a = 0, l_m = 1nm^2$. Temperature increase and dimensionless magnetic field $\Delta T = H_x^m = 0$

	λ_1			λ_2			λ_3		
k	*L*/*h* = 10	*L*/*h* = 30	*L*/*h* = 100	*L*/*h* = 10	*L*/*h* = 30	*L*/*h* = 100	*L*/*h* = 10	*L*/*h* = 30	*L*/*h* = 100
0	10.18390	10.33241	10.34964	38.95773	41.10821	41.37905	57.09278	91.70258	93.03499
0.1	10.18281	10.33240	10.34962	38.95308	41.10818	41.37897	57.07359	91.70246	93.03478
0.3	10.17727	10.33233	10.34949	38.92949	41.10806	41.37852	56.97672	91.70186	93.03358
0.7	10.16477	10.33217	10.34921	38.87602	41.10776	41.37750	56.76055	91.70047	93.03084
1	10.15731	10.33207	10.34904	38.84394	41.10757	41.37689	56.63305	91.69958	93.02921
2	10.14270	10.33186	10.34871	38.78076	41.10716	41.37567	56.38671	91.69773	93.02594
5	10.13048	10.33167	10.34842	38.72753	41.10678	41.37462	56.18391	91.69608	93.02315
10	10.12690	10.33161	10.34833	38.71187	41.10667	41.37431	56.12505	91.69557	93.02232

is observed that the frequency parameter increases with increasing the beam aspect ratio and vibration modes while insignificant effect of beam aspect ratio and vibration mode on $\Delta\lambda_i$ is observed; almost same values are detected for all vibration modes at all values of *L*/*h*.

Considering CMC FGM nanobeams, increasing the material graduation parameter results in increasing the nondimensional frequency parameters due to increasing the overall system stiffness for all vibration modes and beam aspect ratio, see Table 5. The absolute relative percentage change in the nondimensional frequency parameter between k = 0 to k = 10; $\%\Delta\lambda_{i(k=0\rightarrow k=10)}$ reaches 3%. Additionally, this percentage is insignificantly affected by either vibration mode or beam aspect ratio.

On contrary to that observed in CMC FGM beams, increasing the material graduation parameter for sigmoid FGM results in decreasing the nondimensional frequency parameter due to decreasing the overall system stiffness. On the other hand, smaller values of $\%\Delta\lambda_{i(k=0\rightarrow k=10)}$ are detected compared with those observed for MCM and CMC beams; it reaches 1.7% at *L*/*h* = 10 for the third vibration mode.

Neglecting the microstructure effect, the introduction of the nonlocality effect results in material softening thus smaller values of the nondimensional frequency parameters are detected compared with the corresponding classical cases for all functionally graded materials (FGM) distributions; as indicated in Tables 7-9. On the other hand, insignificant effect is observed for the nonlocal parameter on $\%\Delta\lambda_i$; almost the same percentage of the classical cases are detected.

On the other hand, if the nonlocality effect is neglected and considering the microstructure effect only, variations of the nondimensional frequency parameter with *k* for different FGM material distributions are shown in Tables 10 and 11. It is observed that incorporating the microstructure effect increases the overall system stiffness consequently larger values of the nondimensional frequency parameters are obtained compared with the corresponding classical cases for all material distributions. Also $\%\Delta\lambda_i$ is insignificantly affected by incorporating the microstructure length scale parameter.

5.1.2 Magnetic field effects

The dependency of the frequency parameters on the magnetic field for the first three vibration modes at different beam aspect ratios for MCM and CMC FGM distributions is respectively depicted in Tables 13 and 14. It is observed that the introduction of the magnetic effect decreases the system flexibility thus large values of the nondimensional frequency parameters are produced for all beam aspect ratios at all vibration modes. The relative percentage difference of the nondimensional frequency parameter, $\%\Delta\lambda_i = \left[\frac{(\lambda_i)_{H=5}-(\lambda_i)_{H=0}}{(\lambda_i)_{H=0}}\right]\times 100$ significantly affected by

Table 13 Comparisons of dimensionless frequencies of MCM FGM nanobeams for dimensionless magnetic field and *L*/*h*, nonlocal and size parameters:$e_0a = l_m = 0$. Temperature increase $\Delta T = 0$, k = 0.5

	λ_1			λ_2			λ_3		
H_x^m	*L*/*h* = 10	*L*/*h* = 30	*L*/*h* = 100	*L*/*h* = 10	*L*/*h* = 30	*L*/*h* = 100	*L*/*h* = 10	*L*/*h* = 30	*L*/*h* = 100
0	9.2799	9.4115	9.4288	35.5255	37.4461	37.6895	75.0304	83.5203	84.73654
1	9.9908	11.4017	15.0690	36.2722	39.5903	44.4218	75.8096	85.7060	91.77803
2	10.6544	13.0926	19.1115	37.0038	41.6241	50.2585	76.5809	87.8372	98.31539
3	11.2790	14.5889	22.4371	37.7212	43.5631	55.4837	77.3444	89.9181	104.4433
4	11.8707	15.9453	25.3306	38.4253	45.4195	60.2575	78.1005	91.9518	110.2350
5	12.4344	17.1951	27.9259	39.1166	47.2027	64.6813	78.8492	93.9415	115.7335

Table 14 Comparisons of dimensionless frequencies of CMC FGM nanobeams for dimensionless magnetic field and *L*/*h*, nonlocal and size parameters:$e_0a = l_m = 0$. Temperature increase $\Delta T = 0$, k = 0.5

	λ_1			λ_2			λ_3		
H_x^m	*L*/*h* = 10	*L*/*h* = 30	*L*/*h* = 100	*L*/*h* = 10	*L*/*h* = 30	*L*/*h* = 100	*L*/*h* = 10	*L*/*h* = 30	*L*/*h* = 100
0	10.0680	10.2172	10.2356	38.4655	40.6416	40.9219	80.9952	90.6123	91.9896
1	10.6431	11.8461	14.9875	39.0703	42.3694	46.4097	81.6326	92.3698	97.6723
2	11.1886	13.2766	18.5612	39.6659	44.0294	51.3170	82.2650	94.0944	103.0458
3	11.7088	14.5675	21.5493	40.2527	45.6293	55.7916	82.8926	95.7880	108.1508
4	12.2068	15.7526	24.1716	40.8310	47.1749	59.9343	83.5154	97.4521	113.0288
5	12.6853	16.8547	26.5367	41.4013	48.6714	63.8086	84.1337	99.0883	117.7001

Table 15 Comparisons of dimensionless frequencies of MCM FGM nanobeams for temperature increase ΔT and *L*/*h*, nonlocal and size parameters and dimensionless magnetic field: $e_0a = l_m = H_x^m = 0$, k = 0.5

	λ_1			λ_2			λ_3		
ΔT	*L*/*h* = 5	*L*/*h* = 10	*L*/*h* = 20	*L*/*h* = 5	*L*/*h* = 10	*L*/*h* = 20	*L*/*h* = 5	*L*/*h* = 10	*L*/*h* = 20
0	8.8813	9.2799	9.3907	30.9667	35.5255	37.1199	59.5023	75.0304	81.9531
25	8.8327	9.0816	8.5659	30.9176	35.3310	36.3264	59.4486	74.8369	81.1691
50	8.7814	8.8718	7.6243	30.8637	35.1256	35.4876	59.3876	74.6287	80.3448
75	8.7272	8.6500	6.5161	30.8049	34.9090	34.6001	59.3195	74.4056	79.4792
100	8.6702	8.4151	5.1348	30.7413	34.6811	33.6605	59.2442	74.1677	78.5709
125	8.6104	8.1661	3.1384	30.6728	34.4418	32.6645	59.1618	73.9148	77.6187

the magnetic field, this percentage increases with increasing beam aspect ratio while smaller percentages are detected at higher vibration modes. At the first vibration mode, $\%\Delta\lambda_1$ reaches 34% for MCM and 26% for CMC at *L*/*hv* = 10 these percentage increases and reach 196.18% for MCM and 159.26% for CMC at at *L*/*h* = 100. On the other hand, these percentage are decreased in the third mode and reach 5.09% for MCM and 3.9% for CMC at *L*/*h* = 10 and 36.6% for MCM and 28% for CMC at *L*/*h* = 100.

5.1.3 Temperature effect

Variations of the nondimensional frequency parameter on the temperature rise, ΔT at different beam aspect ratios for different FGM material distributions are illustrated in Tables 15-17. Generally, increasing temperature results in material relaxation leading to decreasing the non-dimensional frequency parameters. Comparing the different FGM materials distributions, CMC distribution results in higher values of the nondimensional frequency parameter due its higher stiffness compared with both MCM and sigmoid distribution.

The relative percentage difference of the nondimensional frequency parameter, $\%\Delta\lambda_i = \left[\frac{(\lambda_i)_{\Delta T=125}-(\lambda_i)_{\Delta T=0}}{(\lambda_i)_{\Delta T=0}}\right]\times 100$ greatly affected by the temperature rise, this percentage increases with increasing beam aspect ratio, (*L*/*h*) and decreases with increasing vibration mode. At the first vibration mode, $\%\Delta\lambda_1$ reaches 3% for MCM, 2% for CMC, and 5% for Sigmoid at *L*/*h* = 10 these percentage increases and reach 67% for MCM, 55% for CMC, and 73% for Sigmoid at *L*/*h* = 100. On the other hand, these percentage are decreased in the third mode and reach 0.6% for MCM, 0.4 for CMC and 1.6% for sigmoid at *L*/*h* = 10 and 5.3% for MCM, 3.6% for CMC, and 8.8% for sigmoid at *L*/*h* = 100.

5.1.4 Coupled thermomagnetic effect on the frequency parameters

Dependencies of the nondimensional frequency parameters on the temperature rise for the lowest three

Table 16 Comparisons of dimensionless frequencies of CMC FGM nanobeams for temperature increase ΔT and L/h, nonlocal and size parameters and dimensionless magnetic field: $e_0a = l_m = H_x^m = 0$, $k = 0.5$

	λ_1			λ_2			λ_3		
ΔT	$L/h = 5$	$L/h = 10$	$L/h = 20$	$L/h = 5$	$L/h = 10$	$L/h = 20$	$L/h = 5$	$L/h = 10$	$L/h = 20$
0	9.6163	10.0680	10.1934	33.3048	38.4655	40.2721	63.4654	80.9952	88.8368
25	9.5776	9.9215	9.6045	33.2585	38.3105	39.6860	63.4094	80.8266	88.2370
50	9.5386	9.77058	8.9647	33.2132	38.1546	39.0822	63.3550	80.6598	87.6281
75	9.4994	9.6150	8.2623	33.1688	37.9979	38.4603	63.3023	80.4947	87.0098
100	9.4601	9.4548	7.4801	33.1255	37.8404	37.8193	63.2513	80.3314	86.3819
125	9.4205	9.2895	6.5896	33.0831	37.6821	37.1583	63.2019	80.1699	85.7445

Table 17 Comparisons of dimensionless frequencies of SIGMOID FGM nanobeams for temperature increase ΔT and L/h, nonlocal and size parameters and dimensionless magnetic field: $e_0a = l_m = H_x^m = 0$, $k = 0.5$

	λ_1			λ_2			λ_3		
ΔT	$L/h = 5$	$L/h = 10$	$L/h = 20$	$L/h = 5$	$L/h = 10$	$L/h = 20$	$L/h = 5$	$L/h = 10$	$L/h = 20$
0	9.2081	9.6974	9.8048	26.4563	37.0913	38.8474	32.2207	54.2176	85.7885
25	9.1220	9.3513	8.8956	26.4626	36.7416	37.4608	32.1261	54.2193	84.4012
50	9.0324	8.9828	7.8558	26.4654	36.3796	35.9851	32.0284	54.2200	82.9560
75	8.9394	8.5892	6.6244	26.4647	36.0049	34.4089	31.9275	54.2198	81.4501
100	8.8429	8.1668	5.0638	26.4605	35.6171	32.7179	31.8237	54.2185	79.8801
125	8.7427	7.7110	2.6444	26.4528	35.2159	30.8936	31.7167	54.2162	78.2424

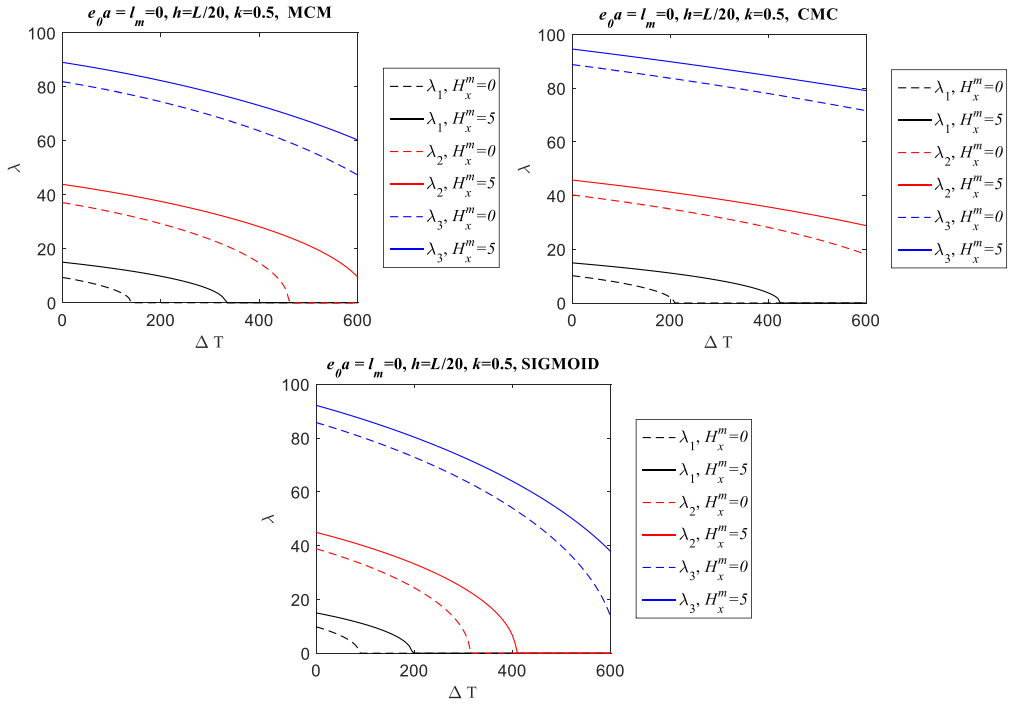

Fig. 2 The effect of the magnetic field intensity for improving the thermal behavior of FGM nanobeams for different material distributions

vibration modes at different values of the nondimensional magnetic field for different FGM distributions for classical and nonclassical analysis are depicted in Fig. 2. As stated previously, incorporating thermal effects results in material relaxation thus decreases the nondimensional frequency parameters for all material distribution at all vibration modes. Moreover, the introduction of the magnetic effect increases the system stiffness which results in larger values of the nondimensional frequency parameters. On the other hand, incorporating the coupled thermomagnetic effect results in decreasing the nondimensional frequency decreasing rate with temperature especially at lower

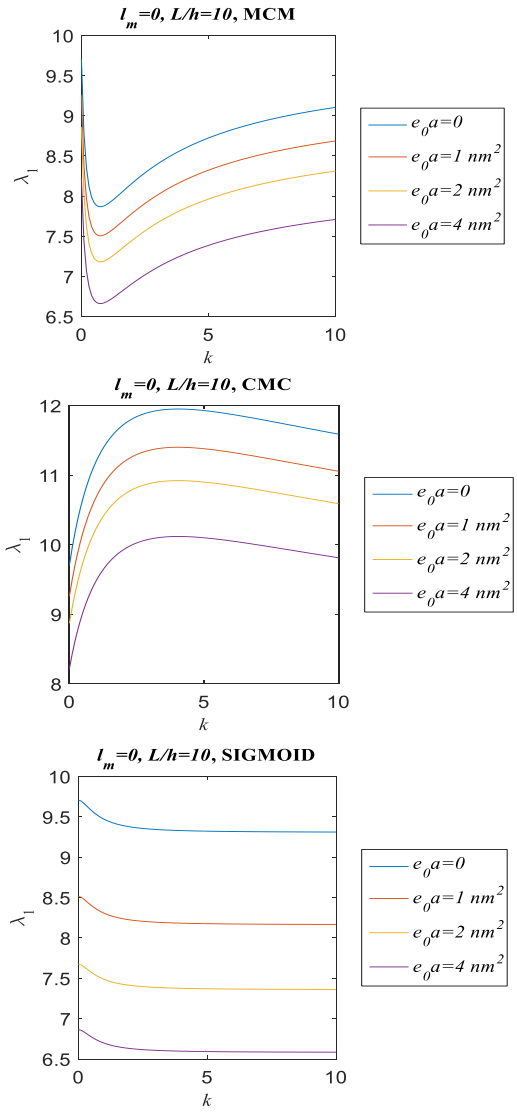

Fig. 3 Comparisons of fundamental frequencies versus k for L/h = 10 for different nonlocality parameter, $e_0a = 0,1,2,4\ nm^2$ at $l_m = 0\ nm^2$ at $H_x^m \Delta T = 0$ for different FGM distributions

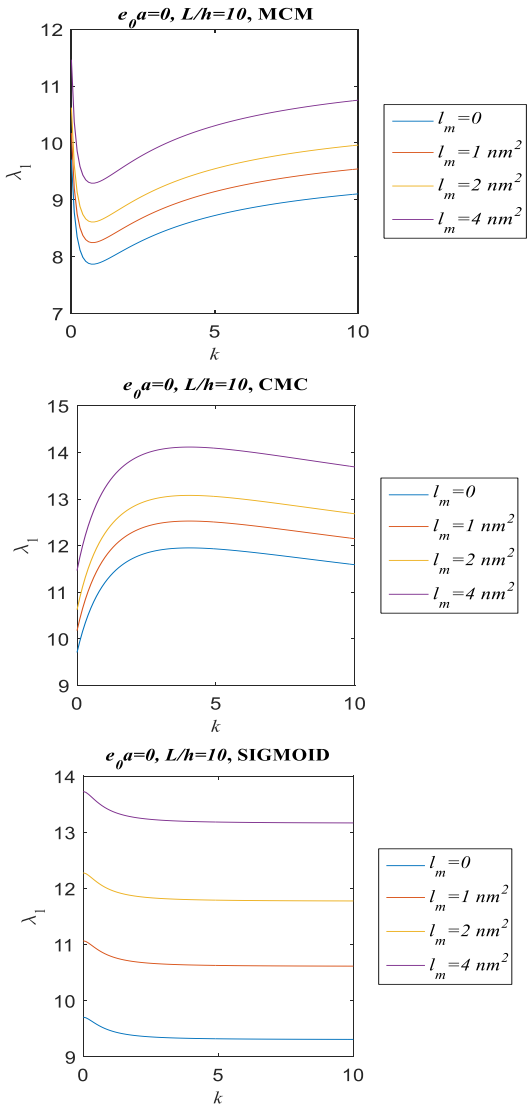

Fig. 4 Comparisons of fundamental frequencies versus k for L/h= 10, and nonlocality parameter, $e_0a = 0\ nm^2$ for different size parameters; $l_m = 0,1,2,4\ nm^2$ at $H_x^m = \Delta T = 0$ for different FGM distributions

vibration modes and high temperature rise. Comparing the FGM distributions, sigmoid FGM produces a larger decreasing rate in the nondimensional frequency parameters compared to both CMC and MCM FGM distributions. On the other hand, slower decreasing rate is predicted for CMC FGM beams compared to both MCM and sigmoid FGM distributions.

5.1.5 Effect of nonlocal and material size parameters

Variations of the fundamental nondimensional frequency parameter with the material graduation index, k for different FGM distributions at different nonlocal and size parameters are respectively depicted in Figs. 3 and 4. Generally, increasing the material graduation index results in increasing the nondimensional frequency parameters for CMC FGM beams while this trend is reversed for sigmoid FGM beams. On the other hand, considering MCM FGM, increasing k from $0 < k < 1$ results in decreasing λ_1 and then it is increased with increasing k for $k > 1$. Additionally, incorporating the nonlocal effect only results in material softening which reduces the fundamental nondimensional frequency parameter. On the other hand, the introduction of the material size parameter results in material hardening thus larger values of the fundamental nondimensional frequency parameters is detected.

5.2 Forced vibration response under moving load

The proposed methodology is applied to study and analyze the forced vibration response of functionally graded simply supported nanobeam under moving load. The beam has the following geometrical characteristics; $L = 10^{-9}\ m$, $b = h$, $h = L/10$ otherwise stated. The beam is assumed to be made of FGM with the constituents; *SUS* 304 and Si_3Ni_4. Through numerical analysis, the moving load is accepted as 10 nN. The dimensionless velocity parameter, β is defined

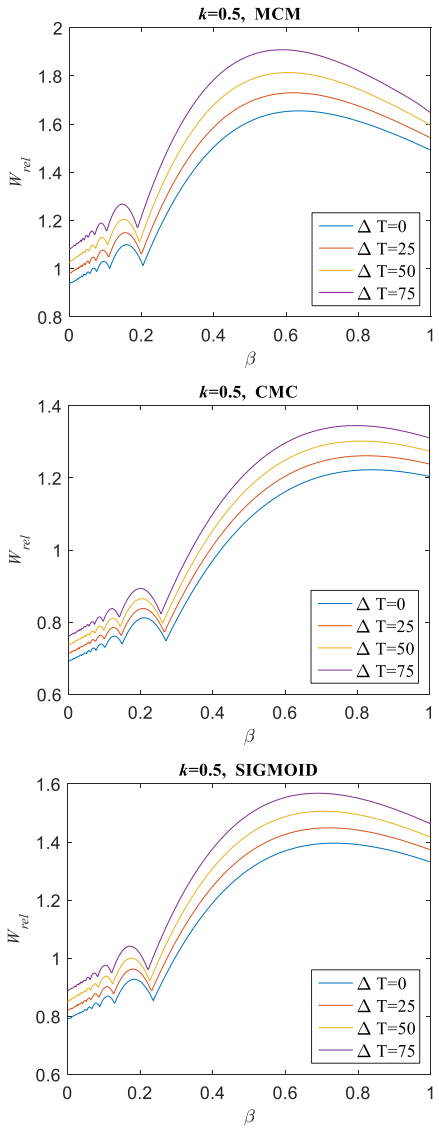

Fig. 5 Comparisons of maximum normalized midspan deflections of MCM, CMC and Sigmoid FGMs versus β for $\Delta T = 0, 25, 50, 75\ K$, power-law exponent k = 0.5, Normalized to displacements of k = 0 at $e_0 a = l_m = H_x^m = 0$

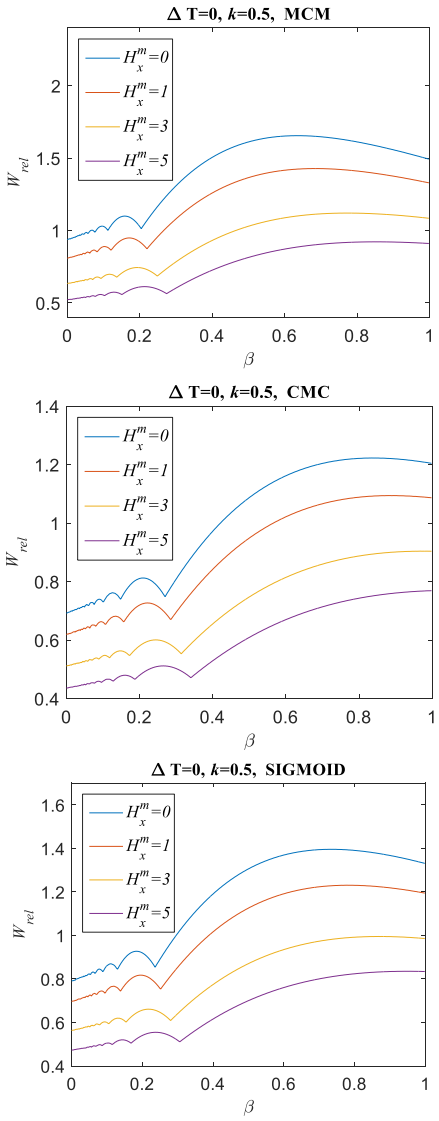

Fig. 6 Comparisons of maximum normalized midspan deflections of MCM, CMC and Sigmoid FGMs versus β for $H_x^m = 0, 1, 3, 5$. power-law exponent k = 0.5, Normalized to displacements of k = 0 at $e_0 a = l_m = \Delta T = 0$

as $\beta = v/v_{crital}$, when β = 1 means the load velocity reaches its first critical speed of the beams. The midspan displacements are normalized by using the static midpoint deflection of the beams with k = 0, $W_{rel} = \frac{W(L/2,t)}{W_{static}(L/2)|_{k=0}}$. To investigate the effect of functionally graded material properties distribution, symmetric MCM, CMC, and sigmoid functionally graded beams are studied and analyzed.

Comparison between variations of the maximum normalized midspan deflections of MCM, CMC and Sigmoid FG nanobeams versus β for different values of temperature rise is depicted in Fig. 5. Due to material relaxation associated with incorporating thermal effect, larger values of the maximum normalized deflection are produced with increasing the temperature rise.

Moreover, it is observed that MCM FGM beam produces larger normalized deflection at all temperature rise compared to both CMC and sigmoid FGM beams. On the other hand, the maximum normalized midspan deflection with larger oscillatory zone $\beta \cong 0.3$ is detected for CMC FG beam while smaller oscillatory zone is produced by MCM FG beam, $\beta \cong 0.2$. Moreover, the temperature rise has insignificant effect on the size of the oscillatory zone; almost the same oscillatory zone is observed for all values of temperature rise. Incorporating the magnetic effect significantly affects variations of the maximum normalized deflection versus the normalized velocity parameter, β, for MCM, CMC, and sigmoid FG beams, as illustrated in Fig. 6. It is noticed that introduction of the magnetic effect results in material hardening thus reduces the material flexibility which results in smaller values of the maximum normalized midspan deflections for all FGMs material properties distributions. Also, the oscillatory zone

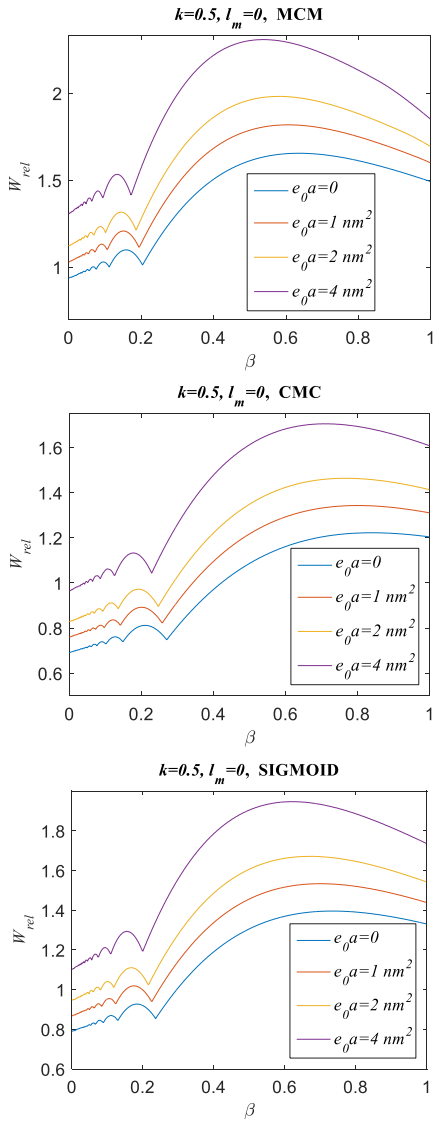

Fig. 7 Comparisons of maximum normalized midspan deflections of MCM, CMC and Sigmoid FGMs versus β for L/h = 10, k = 0.5, and nonlocal parameter, $e_0a = 0, 1, 2, and\ 4\ nm^2$ and size parameters, $l_m = 0\ nm^2$, $H_x^m = \Delta T = 0$

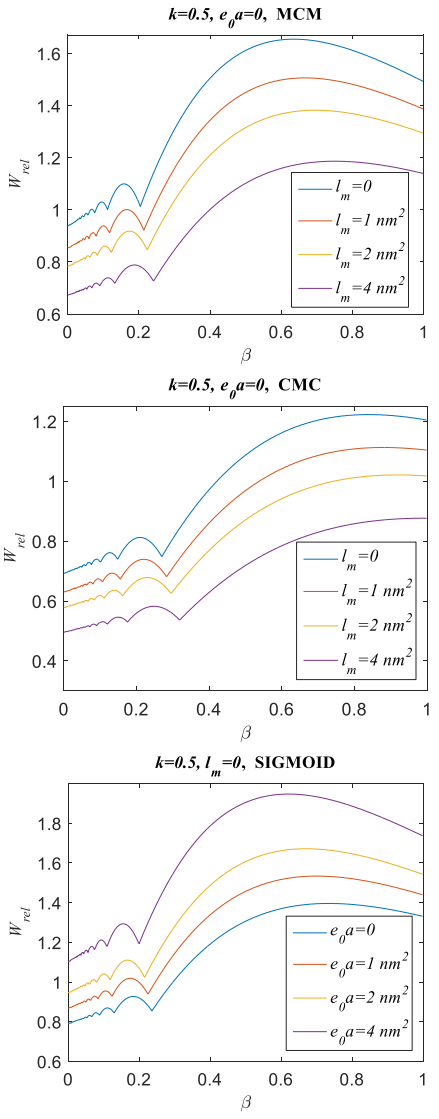

Fig. 8 Comparisons of maximum normalized midspan deflections of MCM, CMC and Sigmoid FGMs versus β for L/h = 10, k = 0.5, and nonlocal parameter, $e_0a = 0\ nm^2$ and size parameters, $l_m = 0, 1, 2, and\ 4\ nm^2$, $H_x^m = \Delta T = 0$

associated with the maximum normalized deflection is affected by incorporating the magnetic field; larger oscillatory zone is detected for all FGMs distributions.

Variations of the maximum normalized deflection with the normalized velocity parameter, β for different FGMs distributions at different values of the nonlocality parameter are shown in Fig. 7. It is observed that neglecting the material microstructure effect, incorporating the nonlocal effect results in material softening which increases the material flexibility thus larger values of the maximum normalized deflection are detected with increasing the nonlocal parameter. Additionally, insignificant effect of the nonlocal parameter on the oscillatory zone associated with the maximum normalized deflection profile for all FGMs distributions.

On the other hand, neglecting the nonlocality effect, introduction of the material size significantly affects the forced vibration time response under moving load. Comparison between the maximum normalized deflection with the nondimensional velocity parameter, β for different FGMs distributions at different values of the material size parameter is illustrated in Fig. 8. It is observed that neglecting the material microstructure effect. It is observed that the introduction of the material size effect results in material hardening which decreases the material flexibility thus smaller values of the maximum normalized deflection are detected with increasing the material size parameter. Also, the material size parameter has insignificant effect on the oscillatory zone associated with the maximum normalized deflection profile for all FGMs distributions.

Variations of the maximum normalized deflection with β at different material graduation index for different FGMs distribution are depicted in Fig. 9. It is noticed that increasing the material graduation index, k significantly

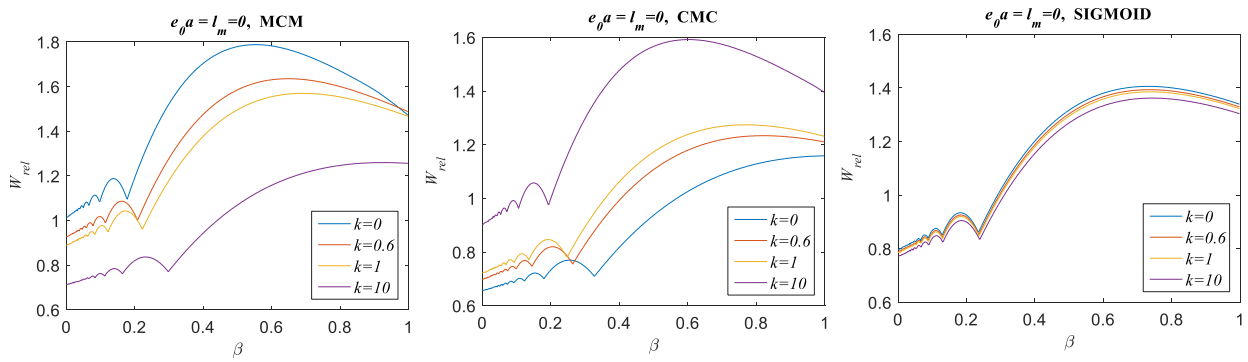

Fig. 9 Comparisons of maximum normalized midspan deflections of MCM, CMC and Sigmoid FGMs versus β for power $-$ law exponent $k = 0, 0.6, 1, 10$ with $e_0a = l_m = \Delta T = H_x^m = 0$

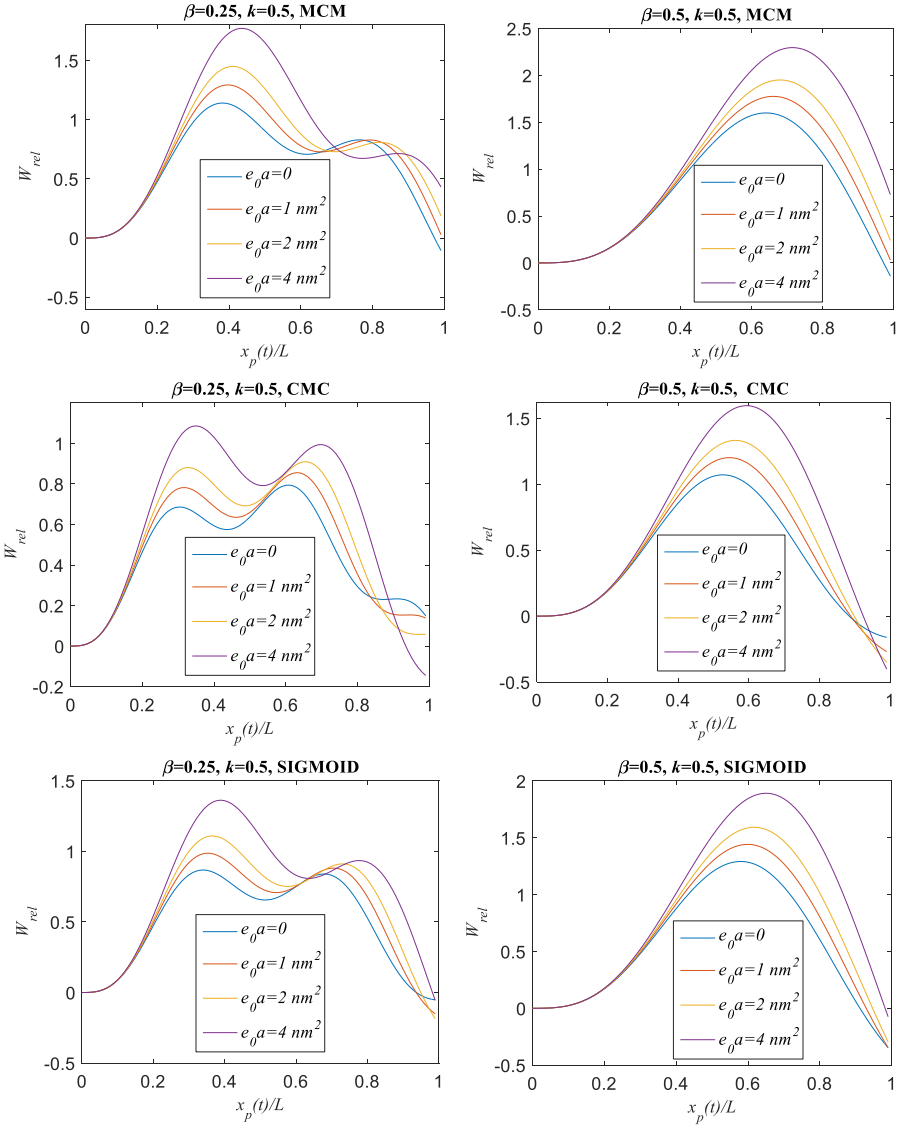

Fig. 10 Comparisons of time histories of the normalized midspan deflections of MCM, CMC, and Sigmoid FGMs for β = 0.25 and 0.5 for power-law exponent, and for $e_0a = 0, 1, 2 \; and \; 4 \; nm^2 \;\; l_m = \Delta T = H_x^m = 0$

affects the maximum nondimensional deflection profile with β for both MCM and CMC FGMs while slight effect is observed for sigmoid FGM. The maximum normalized transverse deflection increases with increasing k for both CMC and sigmoid FGM beams while this trend is reversed for MCM FGM beams. Also, the oscillatory zone associated with the maximum normalized deflection profile increases with increasing k for MCM FGM beam while it is decreased

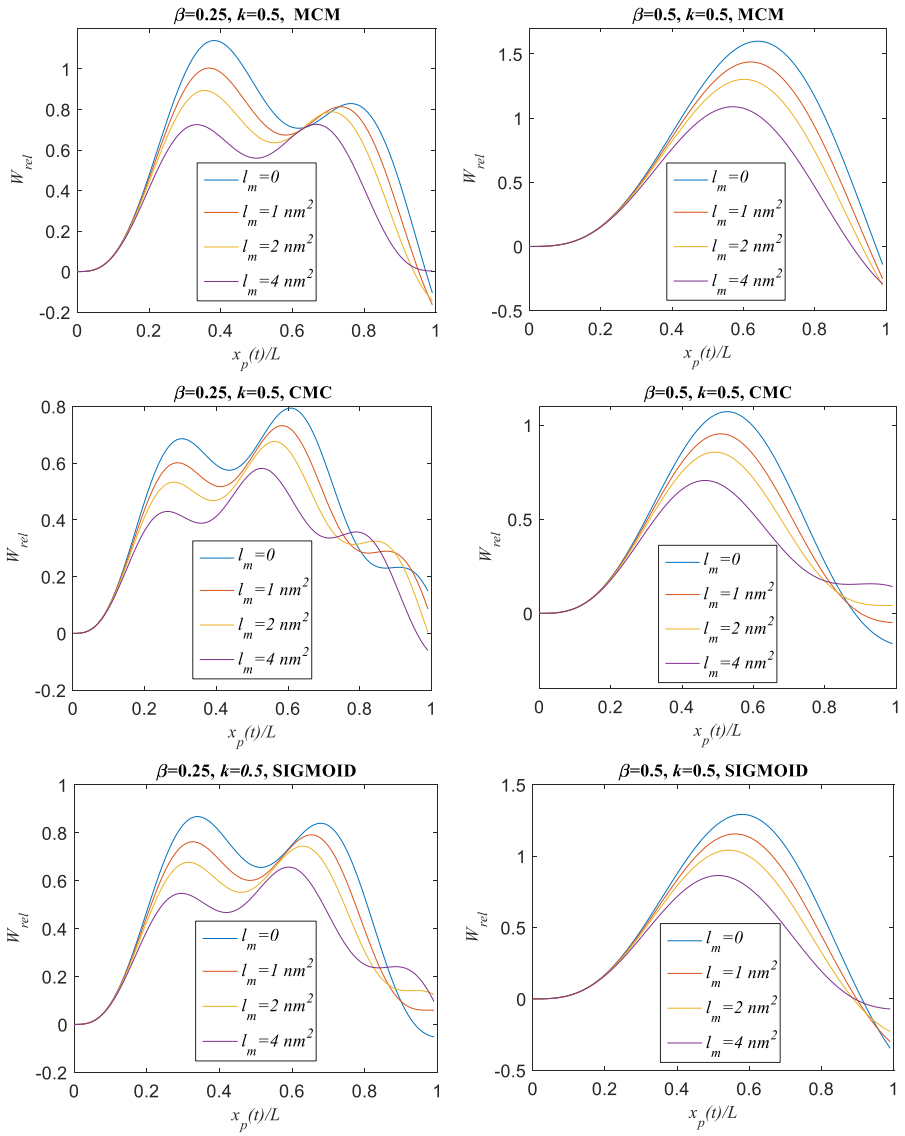

Fig. 11 Comparisons of time histories of the normalized midspan deflections of MCM, CMC, and Sigmoid FGMs for β = 0.25 and 0.5 for power-law exponent, and for $l_m = 0, 1, 2 \; and \; 4 \; nm^2$. $e_0 a = \Delta T = H_x^m = 0$

with increasing k for CMC FGM beam. On the other hand, insignificant effect of k on the size of the oscillatory zone is observed for sigmoid FGM beams.

Variations of the nondimensional transverse deflection profile over the nondimensional coordinate for different FGM distributions at two different values of β at different values of nonlocal parameter are illustrated in Fig. 10. It is observed that smaller values of β; β = 0.25 results in oscillating nondimensional deflection profiles due to the dynamic effect. While smooth profiles are detected at higher values of β; (β = 0.5) for the nondimensional deflection profiles associated with oscillations. Comparing the different FGMs distributions CMC FGM produces the most oscillated profile at β = 0.25 compared with both MCM and sigmoid FGM beams.

Comparisons between the nondimensional deflection profile over the nondimensional coordinate for different FGMs beams at different material size parameters are illustrated in Fig. 11. As stated before, oscillating non-dimensional deflection profile are produced at β = 0.25 for all FGMs distributions while almost quasistatic case is approached at β = 0.5. Also, CMC FGM beams produce the most oscillated nondimensional deflection profile compared with both MCM and sigmoid FGM beams.

Introduction of the magnetic effect significantly affects the nondimensional deflection profile over the normalized coordinate as depicted in Fig. 12. Increasing the magnetic field increasing the overall system stiffness thus smaller deflection are produced. Moreover, at higher values of the magnetic field oscillating profiles are observed especially for CMC FGM beams.

Variations of the nondimensional deflection profile with the normalized coordinate at different values of the temperature rise are depicted in Fig. 13. It is observed that at β = 0.5, almost quasistatic profiles are produced for all material distributions. Moreover, a slight effect of the temperature rise on the nondimensional normalized deflection is observed for all material distributions.

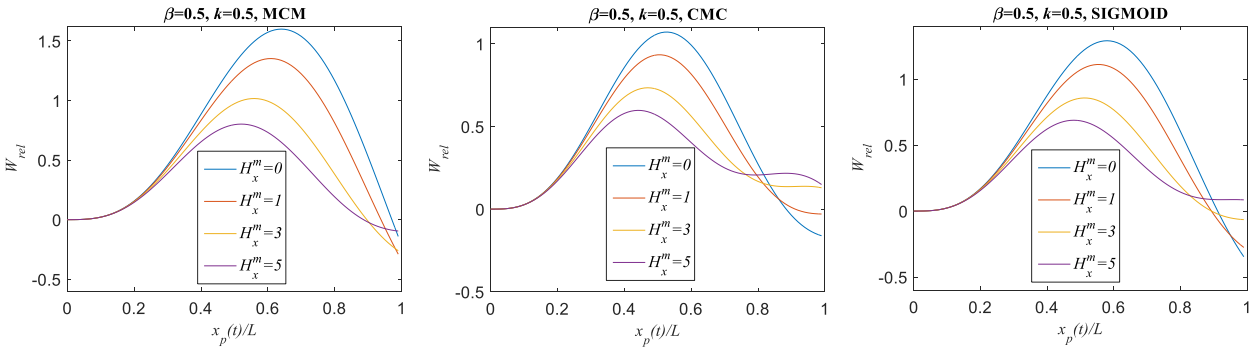

Fig. 12 Comparisons of time histories of the normalized midspan deflections of MCM, CMC, and Sigmoid, FGM nanobeams for β = 0.5 for power-law exponent k = 0.5, and for $H_x^m = 0, 1, 3, 5.\ e_0a\ and\ l_m = \Delta T = 0$

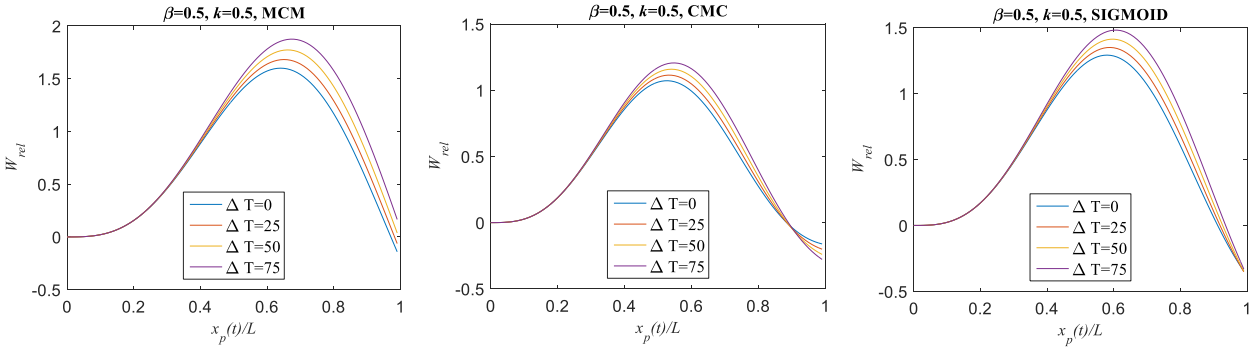

Fig. 13 Comparisons of time histories of the normalized midspan deflections of MCM, CMC, and Sigmoid, FGM nanobeams for β = 0.5 for power-law exponent k = 0.5, and for ΔT = 0, 25, 50, 75. $H_x^m = 0,\ e_0a\ and\ l_m = \Delta T = 0$

6. Conclusions

In the framework of nonlocal strain gradient theory, an analytical methodology is developed to study and analyze the coupled thermomagnetic dynamic behavior of nanobeams under moving load. To investigate the effect of functionally graded material properties distributions, symmetric MCM, CMC, and sigmoid materials are considered. Hamilton's principle is adopted to derive the dynamic governing equations of motion and the associated boundary conditions. Based on Navier approach, an analytical methodology is developed to solve the resulting equations of motion of the FG nanosized beams. Based on the obtained numerical results the following concluding remarks are revealed:

• The nonclassical parameters significantly affect the dynamic behavior of functionally graded nanobeams. The material size parameter results in material hardening while the nonlocal parameter creates material softening effect.

• For the same values of the material size and nonlocal parameters, it was observed that nonlocal parameter was more effective when the effects of the material size parameter and nonlocal parameter were compared.

• Introduction of the magnetic effect creates hardening effect as it adds an additional stiffness this decreases the system flexibility. Consequently, higher values of natural frequencies are obtained while smaller values of the transverse deflections are produced.

• Incorporating the magnetic effect enhances the dynamic transverse deflection performance of the nanobeam

• The free vibration behavior of nanobeams can also be controlled using the stiffening effect of the magnetic field. This makes it useful in resonance control of nanosensors used for measuring in thermal environments.

• Incorporating the thermal effect creates softening effect this increases weakens the strength of the nanobeam to transverse deflection and produces smaller resonant frequencies.

• The desired dynamic thermomagnetic behavior could be adjusted by controlling the power-law exponent, k to provide the most preferable behavior of functionally graded nanobeam.

• Incorporating the shear deformation effect is important especially at the small beam aspect ratio where the shear strains are more affected by the nonclassical parameters.

The proposed model could be used as a ben following model can be used as a benchmark in studying and analyzing the coupled thermomagnetic dynamic behavior of nanoscale functionally graded beam structures.

Acknowledgment

This project was funded by the Deanship of Scientific Research (DSR), King Abdulaziz University, Jeddah, under grant No. (D-180-135-1442). The authors, therefore, gratefully acknowledge DSR technical and financial support.

References

Abdelrahman, A.A., Eltaher, M.A., Kabeel, A.M., Abdraboh, A.M. and Hendy, A.A. (2019), "Free and forced analysis of perforated beams", *Steel Compos. Struct.*, **31**(5), 489-502. https://doi.org/10.12989/scs.2019.31.5.489.

Abdelrahman, A.A. and Eltaher, M.A. (2020), "On bending and buckling responses of perforated nanobeams including surface energy for different beams theories", *Eng. Comput.*, 1-27. https://doi.org/10.1007/s00366-020-01211-8.

Abdelrahman, A. A., Mohamed, N. A. and Eltaher, M. A. (2020a), "Static bending of perforated nanobeams including surface energy and microstructure effects", *Eng. Comput.*, 1-21. https://doi.org/10.1007/s00366-020-01149-x.

Abdelrahman, A.A., Abd-El-Mottaleb, H.E. and Eltaher, M.A. (2020b), "On bending analysis of perforated microbeams including the microstructure effects", *Struct. Eng. Mech.*, **76**(6), 765-779. https://doi.org/10.12989/sem.2020.76.6.765.

Abdelrahman, A.A., Esen, I., Özarpa, C. and Eltaher, M.A. (2021a), "Dynamics of perforated nanobeams subject to moving mass using the nonlocal strain gradient theory", *Appl. Math. Model.*, **96**, 215-235. https://doi.org/10.1016/j.apm.2021.03.008.

Abdelrahman, A.A., Esen, I. and Eltaher, M.A. (2021b), "Vibration response of timoshenko perforated microbeams under accelerating load and thermal environment", *Appl. Math. Comput.*, **407**, 126307. https://doi.org/10.1016/j.amc.2021.126307.

Abdelrahman, A.A., Esen, I., Özarpa, C., Shaltout, R., Eltaher, M.A., and Assie, A.E, (2021c), "Dynamics of perforated higher order nanobeams subject to moving load using the nonlocal strain gradient theory", *Smart Struct. Syst.*, **28**(4), 515-533. https://doi.org/10.12989/sss.2021.28.4.515.

Abo-Bakr, R.M., Eltaher, M.A. and Attia, M.A. (2020), "Pull-in and freestanding instability of actuated functionally graded nanobeams including surface and stiffening effects", *Eng. Comput.*, 1-22. https://doi.org/10.1007/s00366-020-01146-0.

Abo-bakr, H.M., Abo-bakr, R.M., Mohamed, S.A. and Eltaher, M.A. (2021a), "Multi-objective shape optimization for axially functionally graded microbeams", *Compos. Struct.*, **258**, 113370. https://doi.org/10.1016/j.compstruct.2020.113370.

Abo-Bakr, R.M., Abo-Bakr, H.M., Mohamed, S.A. and Eltaher, M.A. (2021b), "Optimal weight for buckling of FG beam under variable axial load using Pareto optimality", *Compos. Struct.*, **258**, 113193. https://doi.org/10.1016/j.compstruct.2020.113193.

Ahn, J. and Rail, Z. (2021), "A rod-beam system with dynamic contact and thermal exchange condition", *Appl. Math. Comput.*, **388**, 125542. https://doi.org/10.1016/j.amc.2020.125542.

Al-shujairi, M. and Mollamahmutoğlu, Ç. (2018), "Buckling and free vibration analysis of functionally graded sandwich micro-beams resting on elastic foundation by using nonlocal strain gradient theory in conjunction with higher order shear theories under thermal effect", *Compos. Part B Eng.*, **154**, 292-312. https://doi.org/10.1016/j.compositesb.2018.08.103.

Alizadeh Hamidi, B., Hosseini, S.A., Hassannejad, R. and Khosravi, F. (2020), "An exact solution on gold microbeam with thermoelastic damping via generalized Green-Naghdi and modified couple stress theories", *J. Therm. Stress.*, **43**(2), 157-174. https://doi.org/10.1080/01495739.2019.1666694.

Arani, A.G. and Jalaei, M.H. (2017), "Investigation of the longitudinal magnetic field effect on dynamic response of viscoelastic graphene sheet based on sinusoidal shear deformation theory", *Physica B*, **506**, 94-104. https://doi.org/10.1016/j.physb.2016.11.004.

Arefi, M., Pourjamshidian, M. and Ghorbanpour Arani, A. (2018). "Nonlinear free and forced vibration analysis of embedded functionally graded sandwich micro beam with moving mass", *J. Sandw. Struct. Mater.*, **20**(4), 462-492. https://doi.org/10.1177/1099636216658895.

Assie, A., Akbaş, Ş.D., Bashiri, A.H., Abdelrahman, A.A. and Eltaher, M.A. (2021), "Vibration response of perforated thick beam under moving load", *Eur. Phys. J. Plus*, **136**(3), 1-15. https://doi.org/10.1140/epjp/s13360-021-01224-2.

Attia, M.A. and Abdelrahman, A.A. (2018), "On vibrations of functionally graded viscoelastic nanobeams with surface effects", *Int. J. Eng. Sci.*, **127**, 1-32. https://doi.org/10.1016/j.ijengsci.2007.04.004.

Avcar, M. (2019), "Free vibration of imperfect sigmoid and power law functionally graded beams", *Steel Compos. Struct.*, **30**(6), 603-615. https://doi.org/10.12989/scs.2019.30.6.603.

Azrar, A., Said, M.B., Azrar, L. and Aljinaidi, A.A. (2019), "Dynamic instability analysis of magneto-electro-elastic beams with uncertain parameters under static and parametric electric and magnetic fields", *Compos. Struct.*, **226**, 111185. https://doi.org/10.1016/j.compstruct.2019.111185.

Barati, M.R. (2017), "Dynamic response of porous functionally graded material nanobeams subjected to moving nanoparticle based on nonlocal strain gradient theory", *Mater. Res. Express*, **4**(11), 115017. https://doi.org/10.1088/2053-1591/aa9765.

Barati, M.R., Faleh, N.M. and Zenkour, A.M. (2019), "Dynamic response of nanobeams subjected to moving nanoparticles and hygro-thermal environments based on nonlocal strain gradient theory", *Mech. Adv. Mater. Struct.*, **26**(19), 1661-1669. https://doi.org/10.1080/15376494.2018.1444234.

Barati, A., Hadi, A., Nejad, M. Z. and Noroozi, R. (2020), "On vibration of bi-directional functionally graded nanobeams under magnetic field", *Mech. Based Des. Struct.*, 1-18. https://doi.org/10.1080/15397734.2020.1719507.

Bensaid, I., Bekhadda, A. and Kerboua, B. (2018), "Dynamic analysis of higher order shear-deformable nanobeams resting on elastic foundation based on nonlocal strain gradient theory", *Adv. Nano Res.*, **6**(3), 279. https://doi.org/10.12989/anr.2018.6.3.279.

Daikh, A.A., Drai, A., Houari M.S.A, and Eltaher, M.A. (2020), "Static analysis of multilayer nonlocal strain gradient nanobeam reinforced by carbon nanotubes", *Steel Compos. Struct.*, **36**(6), 643-656. https://doi.org/10.12989/scs.2020.36.6.64.

Daikh, A.A., Houari, M.S.A. and Eltaher, M.A. (2021a), "A novel nonlocal strain gradient Quasi-3D bending analysis of sigmoid functionally graded sandwich nanoplates", *Compos. Struct.*, **262**, 113347. https://doi.org/10.1016/j.compstruct.2020.113347.

Daikh, A.A., Houari, M.S.A., Karami, B., Eltaher, M.A., Dimitri, R. and Tornabene, F. (2021b), "Buckling analysis of CNTRC curved sandwich nanobeams in thermal environment", *Appl. Sci.*, **11**(7), 3250. https://doi.org/10.3390/app11073250.

Devarajan, B. and Kapania, R.K. (2020), "Thermal buckling of curvilinearly stiffened laminated composite plates with cutouts using isogeometric analysis", *Compos. Struct.*, **238**, 111881. https://doi.org/10.1016/j.compstruct.2020.111881.

Devarajan, B. (2021), "Free vibration analysis of curvilinearly stiffened composite plates with an arbitrarily shaped cutout using isogeometric analysis", *arXiv preprint arXiv:2104.12856*.

Ding, H.X. and She, G.L. (2021), "A higher-order beam model for the snap-buckling analysis of FG pipes conveying fluid", *Struct. Eng. Mech.*, **80**(1), 63-72. https://doi.org/10.12989/sem.2021.80.1.063.

Duraffourg, L. and Arcamone, J. (2015), *Nanoelectromechanical Systems*, John Wiley & Sons, Inc., New Jersey, U.S.A.

Ebrahimi, F. and Barati, M.R. (2016a), "A nonlocal higher-order shear deformation beam theory for vibration analysis of size-dependent functionally graded nanobeams", *Arab. J. Sci. Eng.*, **41**(5), 1679-1690. https://doi.org/10.1007/s13369-015-1930-4.

Ebrahimi, F. and Barati, M.R. (2016b), "Hygrothermal buckling analysis of magnetically actuated embedded higher order functionally graded nanoscale beams considering the neutral

surface position, *J. Therm. Stress.*, **39**(10), 1210-1229. https://doi.org/10.1080/01495739.2016.1215726.

Ebrahimi, F. and Barati, M.R. (2018), "Vibration analysis of smart piezoelectrically actuated nanobeams subjected to magneto-electrical field in thermal environment", *J. Vib. Control*, **24**(3), 549-564. https://doi.org/10.1177/1077546316646239.

Eglin, M., Eriksson, M.A. and Carpick, R.W. (2006), "Microparticle manipulation using inertial forces", *Appl. Phys. Lett.*, **88**(9), 091913. https://doi.org/10.1063/1.2172401.

Eltaher, M.A., Alshorbagy, A.E. and Mahmoud, F.F. (2013a), "Determination of neutral axis position and its effect on natural frequencies of functionally graded macro/nanobeams", *Compos. Struct.*, **99**, 193-201. https://doi.org/10.1016/j.compstruct.2012.11.039.

Eltaher, M.A., Emam, S.A. and Mahmoud, F.F. (2013b), "Static and stability analysis of nonlocal functionally graded nanobeams", *Compos. Struct.*, **96**, 82-88. https://doi.org/10.1016/j.compstruct.2012.09.030.

Eltaher, M.A., Abdelrahman, A.A., Al-Nabawy, A., Khater, M. and Mansour, A. (2014a), "Vibration of nonlinear graduation of nano-Timoshenko beam considering the neutral axis position", *Appl. Math. Comput.*, **235**, 512-529. https://doi.org/10.1016/j.amc.2014.03.028.

Eltaher, M.A., Khairy, A., Sadoun, A.M. and Omar, F.A. (2014b), "Static and buckling analysis of functionally graded Timoshenko nanobeams", *Appl. Math. Comput.*, **229**, 283-295. https://doi.org/10.1016/j.amc.2013.12.072.

Eltaher, M.A., Omar, F.A., Abdalla, W.S., Kabeel, A.M. and Alshorbagy, A.E. (2020a), "Mechanical analysis of cutout piezoelectric nonlocal nanobeam including surface energy effects", *Struct. Eng. Mech.*, **76**(1), 141-151. https://doi.org/10.12989/sem.2020.76.1.141.

Eltaher, M.A., Omar, F.A., Abdraboh, A.M., Abdalla, W.S. and Alshorbagy, A.E. (2020b), "Mechanical behaviors of piezoelectric nonlocal nanobeam with cutouts", *Smart Struct. Syst.*, **25**(2), 219-228. https://doi.org/10.12989/sss.2020.25.2.219.

Eltaher, M.A. and Mohamed, N. (2020), "Nonlinear stability and vibration of imperfect CNTs by doublet mechanics", *Appl. Math. Comput.*, **382**, 125311. https://doi.org/10.1016/j.amc.2020.125311.

Emam, S.A., Eltaher, M.A., Khater, M.E. and Abdalla, W.S. (2018), "Postbuckling and free vibration of multilayer imperfect nanobeams under a pre-stress load", *Appl. Sci.*, **8**(11), 2238. https://doi.org/10.3390/app8112238.

Eringen, A.C. (1983), "On differential equations of nonlocal elasticity and solutions of screw dislocation and surface waves", *J. Appl. Phys.*, **54**(9), 4703-4710. https://doi.org/10.1063/1.332803.

Esen, I. (2019), "Dynamic response of a functionally graded Timoshenko beam on two-parameter elastic foundations due to a variable velocity moving mass", *Int. J. Mech. Sci.*, **153**, 21-35. https://doi.org/10.1016/j.ijmecsci.2019.01.033.

Esen, I., Abdelrahman, A.A. and Eltaher, M.A. (2020), "Dynamics analysis of Timoshenko perforated microbeams under moving loads", *Eng. Comput.*, 1-17. https://doi.org/10.1007/s00366-020-01212-7.

Esen, I., Abdelrhmaan, A.A. and Eltaher, M.A. (2021a), "Free vibration and buckling stability of FG nanobeams exposed to magnetic and thermal fields", *Eng. Comput.*, 1-20. https://doi.org/10.1007/s00366-021-01389-5.

Esen, I., Özarpa, C. and Eltaher, M.A. (2021b), "Free vibration of a cracked FG microbeam embedded in an elastic matrix and exposed to magnetic field in a thermal environment", *Compos. Struct.*, **261**, 113552. https://doi.org/10.1016/j.compstruct.2021.113552.

Esen, I., Eltaher, M.A. and Abdelrahman, A.A. (2021c), "Vibration response of symmetric and sigmoid functionally graded beam rested on elastic foundation under moving point mass", *Mech. Based Des. Struct.*, 1-25. https://doi.org/10.1080/15397734.2021.1904255.

Esen, I., Daikh, A.A. and Eltaher, M.A. (2021d), "Dynamic response of nonlocal strain gradient FG nanobeam reinforced by carbon nanotubes under moving point load", *Eur. Phys. J. Plus*, **136**(4), 1-22. https://doi.org/10.1140/epjp/s13360-021-01419-7.

Hamed, M.A., Eltaher, M.A., Sadoun, A.M. and Almitani, K.H. (2016), "Free vibration of symmetric and sigmoid functionally graded nanobeams", *Appl. Phys. A*, **122**(9), 829. https://doi.org/10.1007/s00339-016-0324-0.

Hamed, M.A., Sadoun, A.M. and Eltaher, M.A. (2019), "Effects of porosity models on static behavior of size dependent functionally graded beam", *Struct. Eng. Mech.*, **71**(1), 89-98. https://doi.org/10.12989/sem.2019.71.1.089.

Hamed, M.A., Abo-bakr, R.M., Mohamed, S.A. and Eltaher, M.A. (2020), "Influence of axial load function and optimization on static stability of sandwich functionally graded beams with porous core", *Eng. Comput.*, **36**(4), 1929-1946. https://doi.org/10.1007/s00366-020-01023-w.

Jalaei, M.H., Arani, A.G. and Nguyen-Xuan, H. (2019), "Investigation of thermal and magnetic field effects on the dynamic instability of FG Timoshenko nanobeam employing nonlocal strain gradient theory", *Int. J. Mech. Sci.*, **161**, 105043. https://doi.org/10.1016/j.ijmecsci.2019.105043.

Jalaei, M.H. and Civalek, Ö. (2019), "A nonlocal strain gradient refined plate theory for dynamic instability of embedded graphene sheet including thermal effects, *Compos. Struct.*, **220**, 209-220. https://doi.org/10.1016/j.compstruct.2019.03.086.

Jankowski, P., Żur, K.K., Kim, J., Lim, C.W. and Reddy, J.N. (2021), "On the piezoelectric effect on stability of symmetric FGM porous nanobeams", *Compos. Struct.*, **267**, 113880. https://doi.org/10.1016/j.compstruct.2021.113880.

Jazi, S.H. (2020), "Nonlinear vibration of an elastically connected double Timoshenko nanobeam system carrying a moving particle based on modified couple stress theory", *Arch. Appl. Mech.*, 1-16. https://doi.org/10.1007/s00419-020-01746-8.

Lal, R. and Dangi, C. (2021), "Dynamic analysis of bi-directional functionally graded Timoshenko nanobeam on the basis of Eringen's nonlocal theory incorporating the surface effect", *Appl. Math. Comput.*, **395**, 125857. https://doi.org/10.1016/j.amc.2020.125857.

Le, C.I., Le, N.A.T. and Nguyen, D.K. (2020), "Free vibration and buckling of bidirectional functionally graded sandwich beams using an enriched third-order shear deformation beam element", *Compos. Struct.*, 113309. https://doi.org/10.1016/j.compstruct.2020.113309.

Li, L. and Hu, Y. (2016), "Nonlinear bending and free vibration analyses of nonlocal strain gradient beams made of functionally graded material", *Int. J. Eng. Sci.*, **107**, 77-97. https://doi.org/10.1016/j.ijengsci.2016.07.011.

Lim, C.W., Zhang, G. and Reddy, J.N. (2015), "A higher-order nonlocal elasticity and strain gradient theory and its applications in wave propagation", *J. Mech. Phys. Solids*, **78**, 298-313. https://doi.org/10.1016/j.jmps.2015.02.001.

Lin, F., Tong, L.H., Shen, H.S., Lim, C.W. and Xiang, Y. (2020), "Assessment of first and third order shear deformation beam theories for the buckling and vibration analysis of nanobeams incorporating surface stress effects", *Int. J. Mech. Sci.*, **186**, 105873. https://doi.org/10.1016/j.ijmecsci.2020.105873.

Lu, L., She, G.L., and Guo, X. (2021a), "Size-dependent postbuckling analysis of graphene reinforced composite microtubes with geometrical imperfection", *Int. J. Mech. Sci.*, **199**, 106428. https://doi.org/10.1016/j.ijmecsci.2021.106428.

Lu, L., Wang, S., Li, M., and Guo, X. (2021b), "Free vibration and dynamic stability of functionally graded composite microtubes reinforced with graphene platelets", *Compos. Struct.*, **272**(15),

114231. https://doi.org/10.1016/j.compstruct.2021.114231.

Mahmoud, F.F., Eltaher, M.A., Alshorbagy, A.E. and Meletis, E.I. (2012), "Static analysis of nanobeams including surface effects by nonlocal finite element", *J. Mech. Sci. Technol.*, **26**(11), 3555-3563. https://doi.org/10.1007/s12206-012-0871-z.

Maneshi, M.A., Ghavanloo, E. and Fazelzadeh, S.A. (2018), "Closed-form expression for geometrically nonlinear large deformation of nano-beams subjected to end force", *Eur. Phys. J. Plus*, **133**(7), 1-10. https://doi.org/10.1140/epjp/i2018-12084-0.

Melaibari, A., Khoshaim, A.B., Mohamed, S.A. and Eltaher, M.A. (2020), "Static stability and of symmetric and sigmoid functionally graded beam under variable axial load", *Steel Compos. Struct.*, **35**(5), 671-685. https://doi.org/10.12989/scs.2020.35.5.671.

Mirnezhad, M., Ansari, R. and Falahatgar, S.R. (2020), "Quantum effects on the mechanical properties of fine-scale CNTs: An approach based on DFT and molecular mechanics model", *Eur. Phys. J. Plus*, **135**(11), 1-71. https://doi.org/10.1140/epjp/s13360-020-00878-8.

Najafi, F., Shojaeefard, M.H. and Googarchin, H.S. (2017), "Nonlinear dynamic response of FGM beams with Winkler–Pasternak foundation subject to noncentral low velocity impact in thermal field", *Compos. Struct.*, **167**, 132-143. http://doi.org/10.1016/j.compstruct.2017.01.063.

Nguyen, D.K., Nguyen, Q.H., Tran, T.T. and Bui, V.T. (2017), "Vibration of bi-dimensional functionally graded Timoshenko beams excited by a moving load", *Acta Mechanica*, **228**(1), 141-155. https://doi.org/10.1007/s00707-016-1705-3.

Ni, Y., Zhu, S., Sun, J., Tong, Z., Zhou, Z. and Xu, X. (2020), "Analytical buckling solution of magneto-electro-thermo-elastic cylindrical shells under multi-physics fields", *Compos. Struct.*, **239**, 112021. https://doi.org/10.1016/j.compstruct.2020.112021

Rahmani, O. and Jandaghian, A.A. (2015), "Buckling analysis of functionally graded nanobeams based on a nonlocal third-order shear deformation theory", *Appl. Phys. A*, **119**(3), 1019-1032. https://doi.org/10.1007/s00339-015-9061-z.

Rajasekaran, S. and Khaniki, H. B. (2019), "Size-dependent forced vibration of non-uniform bi-directional functionally graded beams embedded in variable elastic environment carrying a moving harmonic mass", *Appl. Math. Model.*, **72**, 129-154. https://doi.org/10.1016/j.apm.2019.03.021.

Reddy, J.N. (2007), "Nonlocal theories for bending, buckling and vibration of beams", *Int. J. Eng. Sci.*, **45**(2-8), 288-307. https://doi.org/10.1016/j.ijengsci.2007.04.004.

Reddy, J.N. and Chin, C.D. (1998), "Thermomechanical analysis of functionally graded cylinders and plates", *J. Therm. Stress.*, **21**(6), 593-626. https://doi.org/10.1080/01495739808956165.

Ren, S., Meng, G., Nie, B., Zhou, L. and Zhao, H. (2020), "A novel stabilized node-based smoothed radial point interpolation method (SNS-RPIM) for coupling analysis of magneto-electro-elastic structures in hygrothermal environment", *Comput. Method Appl. M.*, **365**, 112975. https://doi.org/10.1016/j.cma.2020.112975.

Roudbari, M.A., Jorshari, T.D., Arani, A.G., Lü, C. and Rabczuk, T. (2020), "Transient responses of two mutually interacting single-walled boron nitride nanotubes induced by a moving nanoparticle", *Eur. J. Mech. A Solids*, **82**, 103978. https://doi.org/10.1016/j.euromechsol.2020.103978.

Safaei, B., Ahmed, N.A. and Fattahi, A.M. (2019), "Free vibration analysis of polyethylene/CNT plates", *Eur. Phys. J. Plus*, **134**(6), 271. https://doi.org/10.1140/epjp/i2019-12650-x.

She, G.L., Liu, H.B. and Karami, B. (2021), "Resonance analysis of composite curved microbeams reinforced with graphene-nanoplatelets", *Thin Wall. Struct.*, **160**, 107407. https://doi.org/10.1016/j.tws.2020.107407.

She, G.L. (2021a), "Guided wave propagation of porous functionally graded plates: The effect of thermal loadings", *J. Therm. Stress.*, **44(**10), 1289-1305, https://doi.org/10.1080/01495739.2021.1974323.

Sobhy, M. and Zenkour, A.M. (2018). Magnetic field effect on thermomechanical buckling and vibration of viscoelastic sandwich nanobeams with CNT reinforced face sheets on a viscoelastic substrate. *Compos. Part B Eng.*, **154**, 492-506. https://doi.org/10.1016/j.compositesb.2018.09.011.

Touloukian, Y.S. (1966), "Thermophysical properties of high temperature solid materials, volume 5. nonoxides and their solutions and mixtures, including miscellaneous ceramic materials", Thermophysical and Electronic Properties Information Analysis Center Lafayette, Purdue University, Indiana, U.S.A.

Xie, K., Wang, Y. and Fu, T. (2020), "Nonlinear vibration analysis of third-order shear deformable functionally graded beams by a new method based on direct numerical integration technique", *Int. J. Mech. Mater. Des.*, **16**(4), 839-855. https://doi.org/10.1007/s10999-020-09493-y.

Yayli, M.Ö. (2015a), "Buckling analysis of a rotationally restrained single walled carbon nanotube", *Acta Physica Polonica A*, **127**(3), 678-683. https://doi.org/10.12693/APhysPolA.127.678.

Yaylı, M.Ö. (2015b), "Stability analysis of gradient elastic microbeams with arbitrary boundary conditions", *J. Mech. Sci. Technol.*, **29**(8), 3373-3380. https://doi.org/10.1007/s12206-015-0735-4.

Yayli, M.Ö. (2016a). "Buckling analysis of a microbeam embedded in an elastic medium with deformable boundary conditions", *Micro Nano Lett.*, **11**(11), 741-745. https://doi.org 10.1049/mnl.2016.0257.

Yayli, M.Ö (2016b), "An efficient solution method for the longitudinal vibration of nanorods with arbitrary boundary conditions via a hardening nonlocal approach", *J. Vib. Control*, **24**(11), 2230-2246. https://doi.org/10.1177/1077546316684042.

Yayli, M.Ö. (2018a), "Torsional vibrations of restrained nanotubes using modified couple stress theory", *Microsyst. Technol.*, **24**(8), 3425-3435. https://doi.org/10.1007/s00542-018-3735-3.

Yayli, M.Ö. (2018b), "On the torsional vibrations of restrained nanotubes embedded in an elastic medium", *J. Brazil. Soc. Mech. Sci. Eng.*, **40**(9), 1-12. https://doi.org/10.1007/s40430-018-1346-7.

Yayli, M.Ö. (2018c), "Torsional vibration analysis of nanorods with elastic torsional restraints using non-local elasticity theory", *Micro Nano Lett.*, **13**(5), 595-599.

Yayli, M.Ö. (2019), "Effects of rotational restraints on the thermal buckling of carbon nanotube", *Micro Nano Lett.*, **14**(2), 158-162.

Zhang, Y.Y., Wang, X.Y., Zhang, X., Shen, H.M., and She, G.L. (2021), "On snap-buckling of FG-CNTR curved nanobeams considering surface effects", *Steel Compos. Struct.*, **38**(3), 293-304. https://doi.org/10.12989/scs.2021.38.3.293.

Zhang, X.L., Xu, Q., Zhao, X., Li, Y.H. and Yang, J. (2020), "Nonlinear analyses of magneto-electro-elastic laminated beams in thermal environments", *Compos. Struct.*, **234**, 111524. https://doi.org/10.1016/j.compstruct.2019.111524.

JL